siderably higher than that of h-hep-mice at 3 weeks (1.2 ± 0.1%). Based on these analyses, we concluded that the proliferation rate of h-hepatocytes is higher than the death rate of m-hepatocytes, which resulted in the enlargement of liver in h-hep-mice.

## *Histological Architecture of Sinusoids and Bile Canaliculi in Chimeric Mouse*

Liver sinusoids were histologically examined, because their structures reflect the proliferation status of hepatocytes: their structures are compressed[25] and become vague[26] during vigorous hepatocyte proliferation. r-hep- and h-hep$_{9MM}$ Mice were generated and sacrificed in the proliferation (at 2 and 5 weeks after transplantation for r-hep- and h-hep$_{9MM}$ mice, respectively) and proliferation termination phases (at 5 and 14 weeks for r-hep- and h-hep$_{9MM}$ mice, respectively) for histological analysis (Figure 4). Normal livers from Fischer 344 rats and the 65YF donor were used as normal r- and h-liver controls, respectively. H&E sections clearly showed the single-cell structures of hepatic plates in normal r-livers (Figure 4A) and h-livers (Figure 4J). Sections were stained for type IV collagen, an indicator of the subsinusoidal space,[26] and multidrug resistance-associated protein 2 (MRP2), a maker of the canalicular organic anion transporters.[27] These proteins were localized as expected in normal r-livers (Figure 4, B and C) and h-livers (Figure 4, K and L).

H&E-stained sections from r-hep- and h-hep-mouse livers at 5 and 14 weeks, respectively, showed complete repopulation (Figure 4, G and M, respectively), but their histological features were quite different. h-Hepatocytes were less eosinophilic than r-hepatocytes, as reported previously,[7] and swollen and contained less cytoplasm, with wisps of accumulated glycogen, as described previously.[8] Single-cell plates were rarely observable in the

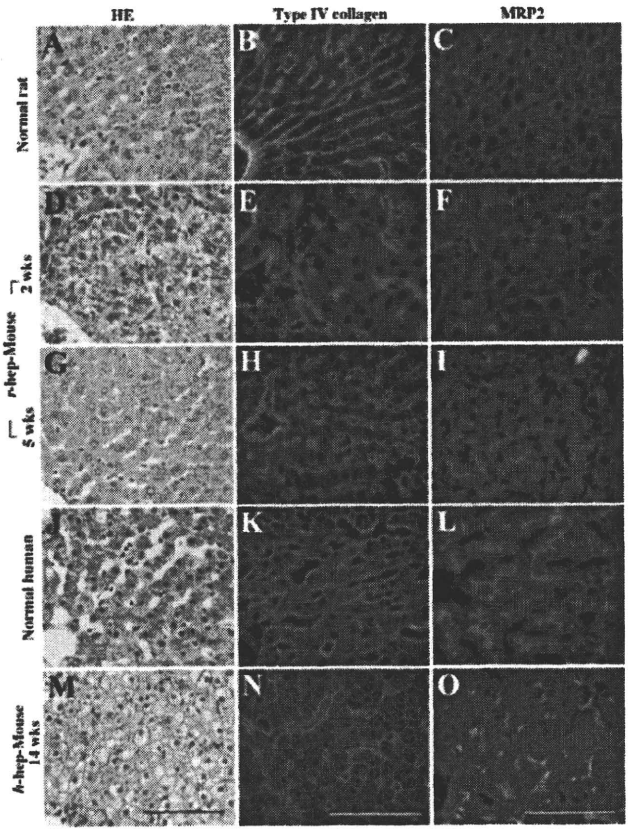


**Figure 4.** Histological characteristics of r-hep- and h-hep-mouse livers. Normal r- and h-livers were obtained from 13-week-old male Fischer 344 rats (**A–C**) and from a 65YF donor (**J–L**), respectively. r-hep-Mice and h-hep-mice were produced as shown in Figure 1. The former were sacrificed at two (proliferation phase, **D–F**) and five weeks (wks) after transplantation (termination phase, **G–I**) and the latter at 14 weeks (termination phase, **M–O**). Liver sections were stained with H&E (**A**, **D**, **G**, **J**, and **M**) and for type IV collagen (red, **B**, **E**, **H**, **K**, and **N**) and MRP2 (red, **C**, **F**, **I**, **L**, and **O**). The sections from rats and r-hep-mice were additionally stained for rRT1A (green, **B**, **C**, **E**, **F**, **H**, and **I**) and those from the human and h-hep-mice for hCK8/18 (green, **K**, **L**, **N**, and **O**) to identify transplanted r- and h-hepatocytes, respectively. The dashed line in **D** shows the boundary between r-hepatocyte (*r*) and m-hepatocyte regions (*m*). Scale bar = 100 μm.

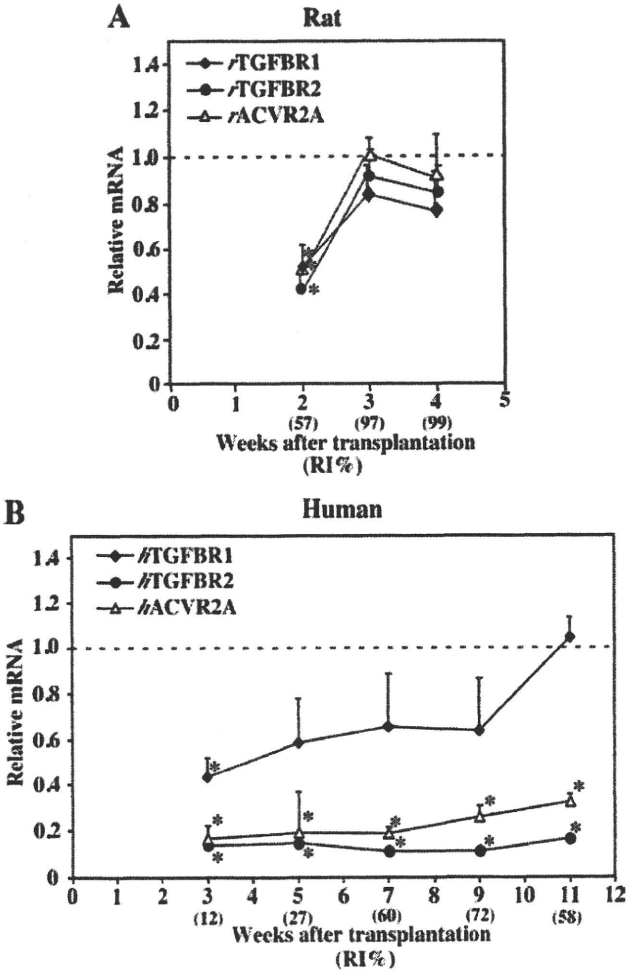


**Figure 5.** Gene expressions of TGFBR1, TGFBR2, and ACVR2A in r-hep- and h-hep-mouse livers. Real-time RT-PCR was performed by using total mRNA isolated from the livers of r-hep- and h-hep$_{9MM}$ mice shown in Figure 1 as templates, and each result was normalized to that of rGAPDH and hGAPDH. Likewise real-time RT-PCR was performed for liver tissues from 13-week-old male rats and those from the 25YF, 28YM, and 61YF human donors as the normal rat and human controls, respectively. mRNA abundance in r- and h-chimeric mice was divided by that of the normal r- and h-livers, respectively, and is shown as relative mRNA abundance (ordinary axis) in **A** for r-hep-mice and in **B** for h-hep-mice. Normal livers in **A** were obtained from three 13-week-old male rats and those in **B** from three donors, 25YF, 28YM, and 61YF. The dotted horizontal lines show the average expression level in normal livers (1.0). The variations of the normalized rTGFBR1, rTGFBR2, rACVR2, hTGFBR1, hTGFBR2, and hACVR2 were 1.0 ± 0.2, 1.0 ± 0.2, 1.0 ± 0.2, 1.0 ± 0.2, 1.0 ± 0.4, and 1.0 ± 0.2, respectively. Values represent the mean ± SD ($n$ = 3). Significant differences compared with normal livers (*$P < 0.05$). "RI%" shows the average RI calculated from three mice. Closed diamond, TGFBR1; closed circle, TGFBR2; and open triangle, ACVR2A.

h-hepatocyte-regions in h-hep-mice at 14 weeks (Figure 4M), and sinusoids were obscure. Type IV collagen immunostains demonstrated multicell-layer-thick hepatic plates (Figure 4N). The MRP2 protein was randomly distributed in the intercellular space (Figure 4O). Similar histological structures were observed in the h-hepatocyte regions at 5 weeks (data not shown). Likewise sinusoidal structures were not distributed in an orderly fashion in the r-hepatocyte regions of r-hep-mice at 2 weeks when r-hepatocytes were in the proliferation phase (Figure 4, D–F), losing vessel continuity along the portal-central axis. However, r-hep-mice at 5 weeks after transplantation regained the normal arrangement of hepatic plates and sinusoids (Figure 4G), which was consistent with the distributions of type IV collagen and MRP2 (Figure 4, H and I). These proteins were located as in normal r-liver, indicating the reconstruction of the resting liver structure with single hepatic plates along the portal-central axis. These results demonstrate that the h-hepatocytes were incapable of reconstructing the resting liver structure even at 14 weeks after transplantation.

The length of the long axis of hepatocytes was determined on H&E-stained sections from r- and h-hep-mice shown in Figure 4 as a measure of size, which showed no significant differences among m (host)-, r-, and h-hepatocytes in chimeric livers: uPA-expressing m-hepatocytes in h-hep$_{9MM}$ mice at 11 weeks after transplantation, 19.5 ± 4.5 $\mu$m ($n$ = 3); uPA-expressing m-hepatocytes in r-hep-mice at 2 weeks, 19.7 ± 4.3 $\mu$m ($n$ = 3); r-hepatocytes in r-mice at 5 weeks, 22.7 ± 2.9 $\mu$m ($n$ = 3); and h-hepatocytes in h-hep-mice at 11 to 14 weeks, 22.5 ± 1.8 $\mu$m ($n$ = 6). This result clearly indicated that the observed enlargement of the h-hep-mouse liver was caused by hyperplasia but not hypertrophy of h-hepatocytes.

## *TGF-β Signaling in r-hep- and h-hep-Mouse Livers*

TGF-β and activin play active roles in the termination of liver regeneration.[14,15,18–20,28] The mRNA expressions of TGFBR1, TGFBR2, and ACVR2A were determined in r-hep-mouse livers at 2, 3, and 4 weeks after transplantation and in h-hep$_{9MM}$ mouse livers at 3, 5, 7, 9, and 11 weeks and compared with those of normal r- and h-liver controls, respectively. In r-hep-mice at 2 weeks (proliferation phase, RI$_{r\text{-}hep}$ = 57%), rTGFBR1, rTGFBR2, and rACVR2A expressions were suppressed to half those of normal r-livers and gradually returned to normal levels at 3 and 4 weeks (termination phase, RI$_{r\text{-}hep}$ = 97 and 99%,

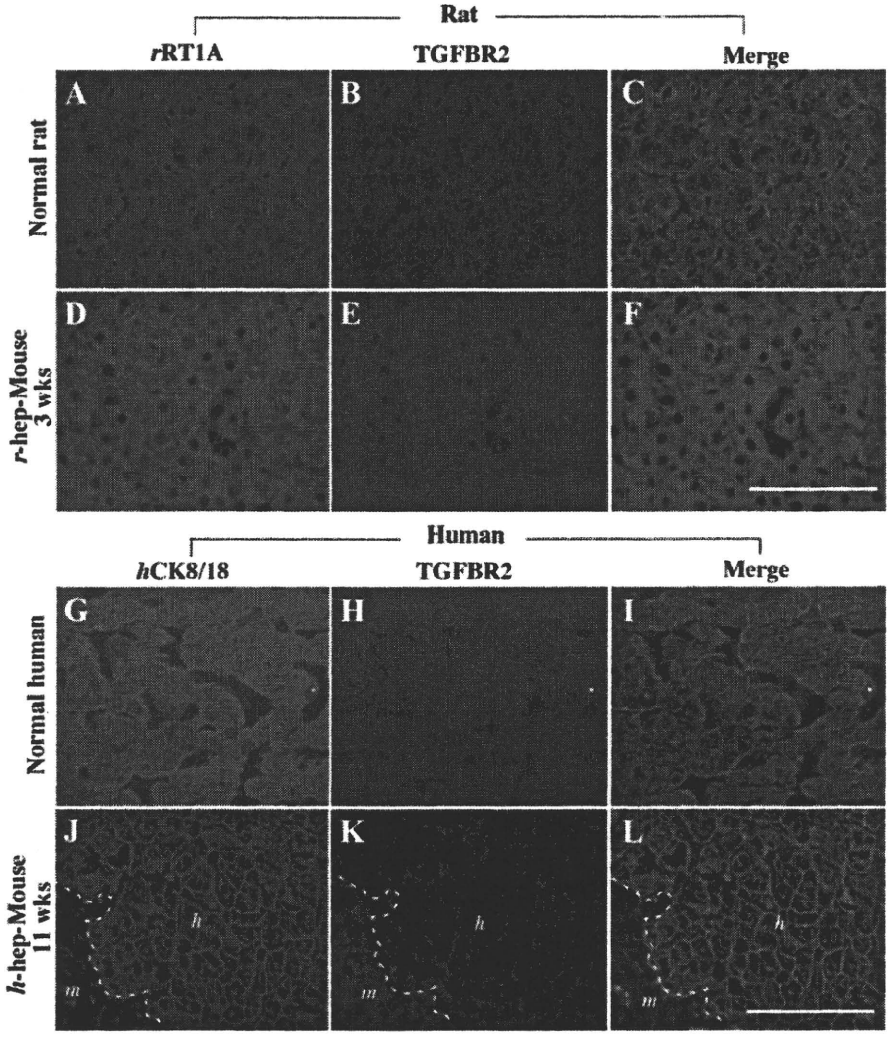


**Figure 6.** Identification and distribution of TGFBR2 in normal and chimeric livers. uPA/SCID mice were transplanted with r- and h-hepatocytes$_{9MM}$ and sacrificed at 3 and 11 weeks after transplantation, respectively, when the transplanted hepatocytes had terminated proliferation. Two series of double immunohistochemical examinations were performed on liver tissues, one for rat series (Rat) shown in **A–F** that contained normal r-liver (Normal rat) shown in **A–C** and r-hep-mouse liver (**D–F**) and the other for the human series (Human) shown in **G–L** that contained 9MM donor liver as control normal h-liver (Normal human, **G–I**) and h-hep-mouse liver (**J–L**). Liver sections of rat series were double-stained for rRT1A for identifying r-hepatocytes (green; **A** and **D**) and TGFBR2 (red; **B** and **E**) and those of human series for hCK8/18 for identifying h-hepatocytes (green; **G** and **J**) and TGFBR2 (red; **H** and **K**). Images **A** and **B**, **D** and **E**, **G** and **H**, and **J** and **K** were merged and are shown in **C**, **F**, **I**, and **L**, respectively. Similar staining results were obtained from three different mice of each series. The **dashed lines** in **J–L** indicate the boundary between h-hepatocyte (*h*) and m-hepatocyte regions (*m*). Scale bar = 100 $\mu$m.

respectively) (Figure 5A) as reported in the regeneration of partial hepatectomized r-liver.[29] In contrast, their expression profiles in h-hep-mouse livers were quite different (Figure 5B). At 3 weeks (proliferation phase, $RI_{h\text{-}hep}$ = 12%), hTGFBR2 and hACVR2A were expressed at levels less than one-third of normal levels; expression remained low throughout the 11-week-long observation period. The suppression of the expression of these genes was reproducible, because similar results were obtained from h-hep-mice generated with another donor (10YF): the ratios of expression levels of hTGFBR2 and hACVR2A in the h-hep-mice at 9 to 11 weeks after transplantation to those in the normal human livers were 0.19 ± 0.05 ($n$ = 3) and 0.19 ± 0.02 ($n$ = 3), respectively. The expression of hTGFBR1 mRNA was high compared with that of these two mRNAs at 3 weeks and gradually increased until reaching the normal levels at 11 weeks.

The expression of TGF-$\beta$ receptor, TGFBR2, was immunohistochemically examined in r- and h-$hep_{9MM}$ mouse livers at 3 and 11 weeks when the mice showed RI = 97 ± 3% ($n$ = 3) and 58 ± 46% ($n$ = 3), respectively, together with staining for rRT1A and hCK8/18 to identify r- and h-hepatocytes, respectively (Figure 6). As with normal r-hepatocytes (Figure 6, A–C), the rRT1A$^+$ r-hepatocytes in r-hep-mice were stained heavily for TGFBR2 (Figure 6, D–F). Likewise normal h-hepatocytes abundantly expressed TGFBR2 (Figure 6, G–I). In contrast, TGFBR2 was hardly detectable in hCK8/18$^+$ h-hepatocytes in h-hep-mice (Figure 6, J–L). The anti-TGFBR2 antibody used was cross-reactive with r- and m-TGFBR2. The TGFBR2$^+$ cells in the m-hepatocyte region seen in Figure 6K were largely m-hepatocytes according to their morphology. Moderately TGFBR2$^+$ cells in the h-hepatocyte region shown in Figure 6K were mostly m-nonparenchymal cells and few h-hepatocytes (Figure 6, K and L). These results indicated that h-hepatocytes in h-hep-mice maintain low sensitivity to TGF-$\beta$, although the expression of TGFBR1 was up-regulated at 11 weeks after transplantation. It is known that TGF-$\beta$ initially binds to TGFBR2, and TGF-$\beta$ signals are transferred through the heterodimers of TGFBR1 and TGFBR2.[16] TGF-$\beta$-expressing cells were identified in liver sections from r- and h-hep-mice during the proliferation and termination phases by double-immunostaining for desmin and TGF-$\beta$ (Figure 7). Compared with the control (Figure 7, A–C; normal liver from wild-type SCID mice), tissues collected from the injured livers of uPA/SCID mice contained abundant desmin$^+$ HSCs that were all heavily expressing TGF-$\beta$ (Figure 7, D–F) as reported previously.[2] Very few desmin$^+$ cells were observed in r-hep-mice at 2 weeks (Figure 7, G–I) or in h-hep-mice at 5 weeks (Figure 7, M–O), suggesting that very few m-HSCs invaded the xenogeneic hepatocyte colonies during the proliferation phase. These cells were all TGF-$\beta^-$. m-HSCs increased in number in xenogeneic hepatocyte colonies from both r- and h-hep-mice, particularly in the former, at 3 and 11 weeks (termination phase), respectively (Figure 7, J and P). During the termination phase, m-HSCs in r-hepatocyte colonies from r-hep-mice were TGF-$\beta^+$ (Figure 7, J–L). However, importantly, m-HSCs in h-hepatocyte colonies of h-hep-mice were TGF-$\beta^-$ (Figure 7, P–R). HSCs that express TGF-$\beta$ should be all m-HSCs in the chimeric mice, because the purity of the transplanted r- or h-hepatocytes was >99%. In r- and h-normal livers, TGF-$\beta^+$-HSCs were rarely observed (data not shown).

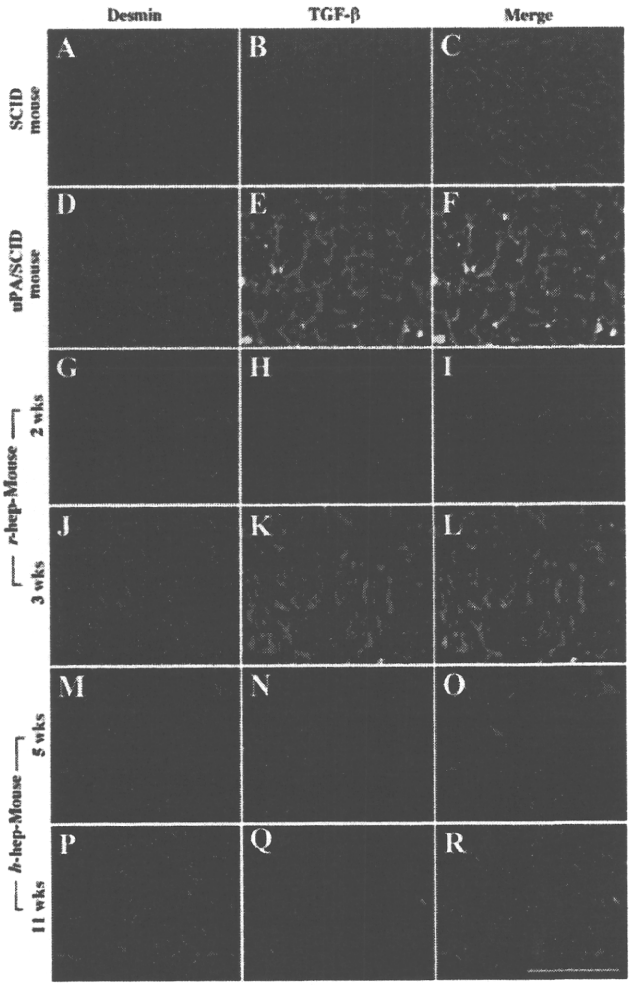


**Figure 7.** Expression and distribution of TGF-$\beta$ in normal and chimeric mouse livers. Livers were removed, respectively, from 3-month-old wild-type SCID mice (**A–C**), 1-month-old uPA/SCID mice (**D–F**, injured region), r-hep-mice at 2 (**G–I**) and three (**J–L**) weeks after transplantation, and h-hep-mice at 5 (**M–O**) and 11 weeks (**P–R**). These livers were cryosectioned and double-immunostained for desmin (**A**, **D**, **G**, **J**, **M**, and **P**, red) and TGF-$\beta$ (**B**, **E**, **H**, **K**, **N**, and **Q**, green). The two sets of photographs are merged and shown in the corresponding panels (**C**, **F**, **I**, **L**, **O**, and **R**) in the **right column**. Serial sections from r- and h-hep-mouse livers were immunostained for rRT1A and hCK8/18 to identify r- and h-hepatocytes, respectively (data not shown). Similar results were obtained from three different mice. Scale bar = 100 $\mu$m.

Smad proteins are major intracellular effectors in both TGFBR and ACVR signaling. The distributions of Smad2/3 were examined on liver sections prepared from r- and h-hep-mice at 3 and at 11 weeks (termination phase of r- and h-hep-mice, respectively), respectively, together with liver tissues from Fischer 344 rats and the 49YM donor as normal controls (Figure 8). The nuclei of normal r-livers (Figure 8, A and B) and h-livers (Figure 8, G and H) were both Smad2$^-$/3$^-$. In contrast, the nuclei of r-hepatocytes in r-hep-mouse were strongly Smad2$^+$/3$^+$ (Figure 8, D and E), supporting the evidence that r-hepatocytes are activated by TGF-$\beta$ from m-HSCs. However, as expected, h-hepatocytes showed little or no Smad2/3 immunoreactivity (Figure 8, J and K), suggesting that

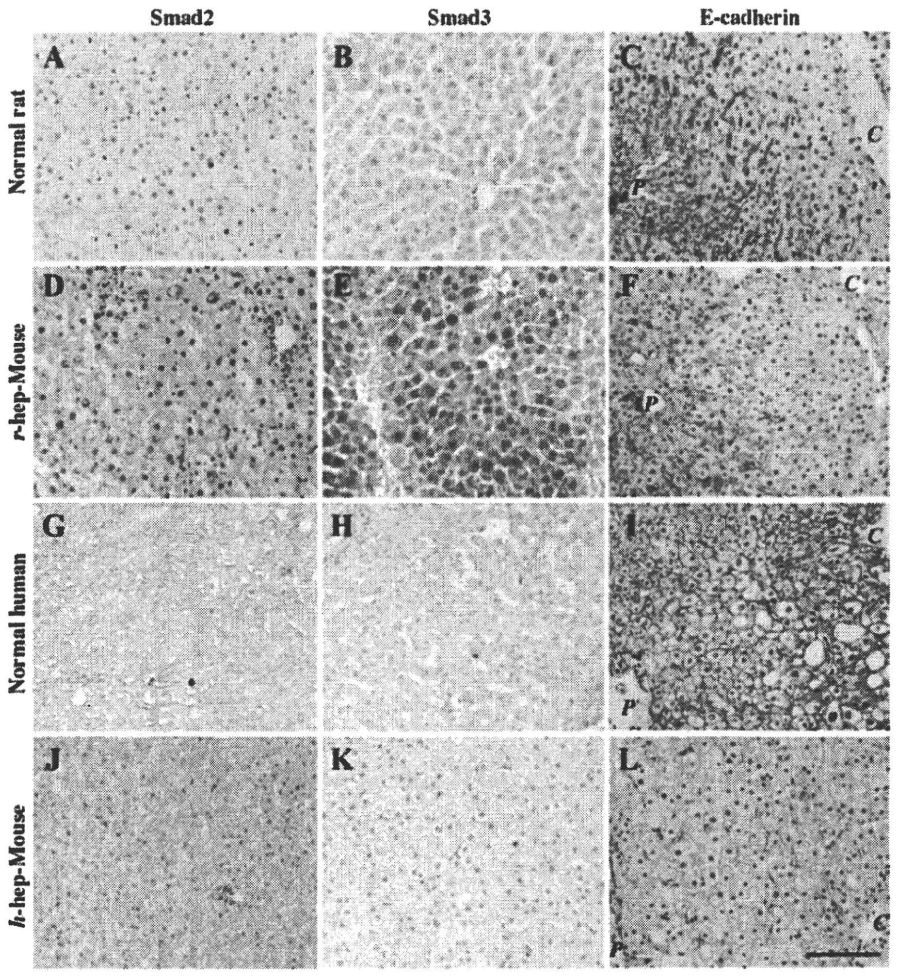


**Figure 8.** Localization of Smad2/3 and E-cadherin in chimeric mouse liver. Livers were obtained from 13-week-old male Fischer 344 rats (**A–C**, Normal rat), normal donors (49YM, 50YM, and 65YF) (**G–I**, Normal human), r-hep-mice at three weeks (**D** and **E**) and five weeks (**F**), and 9MM-h-hep-mice at 11 weeks (**J** and **K**) and 14 weeks (**L**) after transplantation. They were immunostained for Smad2 (**A**, **D**, **G**, and **J**), Smad3 (**B**, **E**, **H**, and **K**), and E-cadherin (**C**, **F**, **I**, and **L**). Positive signals are brown. Histological examinations were individually performed for these livers in each category, and we obtained similar results. Representative photos are shown here. The photos of Normal human were from 49YM liver. In **C**, **F**, **I**, and **L**, *P* and *C* indicate portal and central veins, respectively. Scale bar = 100 μm.

TGF-β and activin signaling was lacking in h-hep-mice. In h-hep mice from another donor (10YF, 9 to 11 weeks after transplantation), the immunohistological results for TGF-β, Smad2, and Smad3 showed the same tendencies as the results shown in Figures 7 and 8 (data not shown), suggesting that the deficiency of TGF-β signaling is not attributed to the possible immaturity because of the young age (9MM) of the donor.

To obtain an additional evidence for the TGF-β signaling deficiency in h-hep-mice, we examined the expression of E-cadherin in the chimeric mouse, which is one of the TGF-β target genes.[30] Normal r-livers expressed the E-cadherin protein in the periportal zone restrictedly (Figure 8C), and a similar distribution pattern was observed in the r-hep-mouse livers (Figure 8F). In contrast to normal r-livers, normal h-livers uniformly and evenly expressed E-cadherin (Figure 8I). Its expression was significantly low in the h-hepatocyte region of the h-hep-mouse liver (Figure 8I) compared with that in the normal h-livers.

## *Participation of m-HSCs in the Donor Hepatocyte Colonies*

As shown in Figure 7, the xenogeneic hepatocyte regions contained fewer m-HSCs than the injured host regions, especially in the proliferation phase. We further investigated this phenomenon using desmin as a HSC marker. The desmin$^+$ cells were scarce in both r- and h-hepatocyte colonies in r-hep-mice at 2 weeks (Figure 9A) and in h-hep-mice at 5 weeks after transplantation (Figure 9B), respectively, compared with the degenerating m-hepatocyte regions that surrounded the corresponding donor cell regions. These xenogeneic hepatocytes were both in the proliferation phase (Figure 1). This paucity of HSCs seemed to be related to the fact that the sinusoids were still under reconstruction (Figure 4E) in r-hep-mouse liver at 2 weeks and in h-hep-mouse liver at 5 weeks (data not shown). HSCs were abundant in r-hepatocyte colonies in r-hep-mice at 3 weeks (termination phase) (Figure 9C), supporting the result of Figure 7J. The HSCs also increased in density in h-hepatocyte colonies of h-hep-mice at 11 weeks (Figure 9D), also supporting the result of Figure 7P. However, the density was apparently lower than that in r-hepatocyte colonies, most probably reflecting the fact that the sinusoids were less developed than in r-hepatocyte colonies in the termination phase (Figure 4N versus Figure 4H, respectively). These desmin$^+$ HSCs were not derived from h-HSCs, because, first the purity of the transplanted h-hepatocytes was >99% and second h-HSCs do not express desmin.[31] The m-HSC-occupied areas (red-colored areas) were measured in the entire normal mouse (wild-type SCID mouse) liver (control) and in the xenogeneic hepatocyte regions of chimeric livers on immunostained sections. The ratios ($R_{HSC}$) of red-colored areas

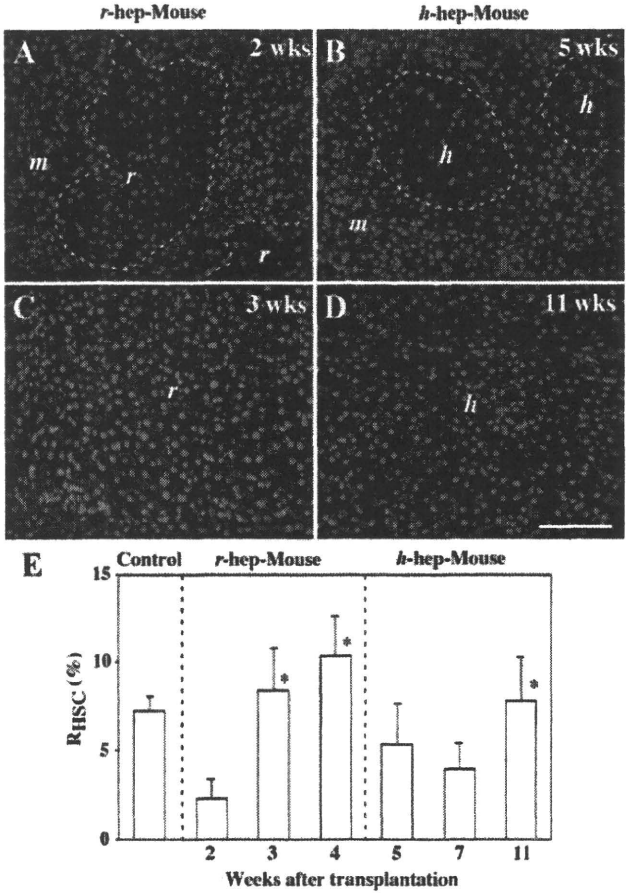


**Figure 9.** Distribution of m-HSCs in r- and h-hep-mice. Liver sections from r-hep-mice at two (proliferation phase, **A**) and three (termination phase, **C**) weeks and from 9MM h-hep-mice at five (proliferation phase, **B**) and 11 (termination phase, **D**) weeks after transplantation were immunostained for desmin (red). The nuclei were stained with Hoechst 33258 (blue). Serial sections from the r-hep- and h-hep-mouse livers were immunostained for rRT1A and hCK8/18 to identify r-and h-hepatocytes, respectively (data not shown), from which the boundary between the host (*m*) and transplanted (*r* or *h*) hepatocyte regions was determined, as indicated by the **dashed lines** in **A** and **B**. Similar results were obtained from three different mice. Scale bar = 100 μm. **E:** Changes in the ratio of desmin$^+$ cells in xenogeneic hepatocyte regions during liver repopulation. Liver sections from 3-month-old wild-type SCID mice (control), r-, and h-hep-mice at the indicated weeks after transplantation were immunostained for desmin. Serial sections were stained with anti-rRT1A and -hCK8/18 antibodies to identify r- and h-hepatocytes, respectively. The ratio ($R_{HSC}$) of desmin$^+$ areas over the measured areas was calculated in the xenogeneic hepatocyte region using NIH imaging software and is expressed as a percentage. Data represent the mean ± SD of desmin$^+$ area per section in a total of 15 randomly selected fields ($n = 3$). **Asterisks** at three and four weeks in the panel for r-hep-mice indicate significant differences versus the value at two weeks. The **asterisk** at 11 weeks in the panel of h-hep-mice indicates a significant difference versus the value at five weeks.

to either the entire liver of SCID mouse or to the xenogeneic region of chimeric liver were calculated and are shown in Figure 9E. The $R_{HSC}$ in normal mice was 7.3 ± 0.8%. In r-hep-mice, the $R_{HSC}$ was 2.3 ± 1.1% at 2 weeks and increased to 10.3 ± 2.3% at 4 weeks. In h-hep-mice, the $R_{HSC}$ was approximately 5% for up to 7 weeks and significantly increased to 7.8 ± 2.4% ($P < 0.01$) at 11 weeks. The $R_{HSC}$ of r-hep-mice at 4 weeks was significantly higher than that of h-hep-mice at 11 weeks ($P < 0.01$).

## *Discussion*

In this study, we compared the repopulation processes between r- and h-hepatocytes in the livers of uPA/SCID mice and showed several physiologically significant differences. The r-hepatocytes rapidly replaced m-hepatocytes to keep a normal $R_{L/B}$, suggesting a repopulation in a strictly regulated manner. The r-hepatocytes expressed TGFBR1/2 mRNAs at lower levels in the proliferation phase and then gradually increased expressions in the termination phase when m-HSCs actively expressed TGF-β. Moreover, Smad2/3 were translocated in r-hepatocyte nuclei, suggesting that TGF-β/TGFBR/Smad signaling normally works as in the terminal phase of mouse liver regeneration.

In the chimeric animal h-hepatocytes were quite different from r-hepatocytes. They proliferated much slowly, requiring approximately four times longer to complete proliferation than r-hepatocytes. The resulting liver showed marked overgrowth compared with a normal m-liver. TGFBR2 and ACVR2A, and TGF-β were not up-regulated in h-hepatocytes and m-HSCs of h-hep-mice, respectively, in the termination phase, indicating the absence of physiologically meaningful signaling between h-hepatocytes and m-HSCs. The density of m-HSCs in h-hepatocyte colonies was lower than that in r-hepatocyte colonies even in the termination phase, which probably reflects the poor development of sinusoids in h-hep-mice, because the multiple hepatic plates would result in the lower volume of the space of Disse than in the liver with single hepatic plates. It has been reported that intimate signaling between hepatocytes and nonparenchymal cells plays an important role in the termination of liver regeneration.[32] Thus, the failure of m-HSCs to express TGF-β could be a cause of liver hyperplasia of h-hep-mice. However, it is appropriate to note here that other factors such as hepatocyte growth factor[33] and bile acids[34] might be involved in the observed hyperplasia.

In TGFBR2 knockout mice, partial hepatectomy resulted in a 1.2-fold increase beyond the normal liver weight because of a compensatory increase in activin A/ACVR2A signaling and persistent activity in the Smad pathway.[20] Unlike in the study cited, the levels of ACVR2A mRNA and Smad proteins remained low through the experimental period in the present study with h-hep-mice. Thus, the lack of both TGF-β and activin signaling may have been partly responsible for the observed overgrowth of hepatocytes. We did not observe any symptoms of carcinogenic transformation in h-hepatocytes (data not shown), although TGFBR2[35] and ACVR2[36] are putative tumor suppressors, suggesting a requirement for additional factor(s) for hepatocarcinogenesis.

Even in the absence of TGF-β/TGFBR signaling, the transplanted h-hepatocytes eventually terminated proliferation. The histological features of sinusoids and canaliculi in mouse liver repopulated by xenogeneic hepatocytes demonstrated that h-hepatocytes did not restore the normal arrangement of single hepatic plates in the resting phase of the liver, but they formed multiple hepatic plates seen in the regenerating liver.[25,26] Thus, it is most likely that h-hepatocytes eventually terminated the proliferation because of contact inhibition within the multiple hepatocyte layers. r-Hepatocytes also formed multiple hepatic plates in the proliferation phase but restored the normal structures of single cell plates along the portal-central axis in the termination phase. It seems that

TGF-β/TGFBR signaling is required for both the formation of single hepatic plates and the normal termination of liver growth. These apparently distinct events (liver growth termination and hepatic plate structuring) should be closely related at the molecular levels, because adhesion molecules such as E-cadherin and β1-integrin are reported as the Smad2/3-mediated TGF-β target genes in liver development.[30] Our results demonstrated that E-cadherin uniformly exists on the hepatocyte surfaces in the normal h-liver, but its expression was quite low in substantial portions of the h-hepatocyte region in the h-hep-mouse liver. It is likely that this expression defect in the cell adhesion molecule results in abnormal hepatocyte plate arrangements. Loss of TGF-β signaling in h-hep-mice might be responsible for the maintenance of multicell-thick hepatic plates after the termination of liver repopulation in the h-hep-mouse livers.

There is the possibility that the observed hyperplasia of h-hepatocytes is the result of a signaling failure between m-cytokine ligands and the corresponding h-receptors. Recently, we showed that h-hepatocytes in h-hep-mice are growth hormone-deficient, because mouse growth hormone does not recognize the human growth hormone receptor of h-hepatocytes.[37] However, we consider that h-hepatocytes would be able to respond to TGF-β if the host m-HSCs secreted it, because there has been no report of species specificity between h- and m-TGF-β. In the present study we clearly demonstrated the coincidence of lack of TGF-β/TGFBR signaling with the hyperplasia of h-hep-mouse liver. However, the direct causality between such signaling and the liver hyperplasia remains to be examined. It is well known that hepatocytes and stellate cells interact with each other through varieties of signaling molecules and together contribute to physiological and pathological changes of liver. Therefore, we conclude that the lack of or weak interaction between h-hepatocytes and m-HSCs, which we have revealed at the histological and gene/protein expression levels, is responsible for the presently observed hyperplasia of h-hep-mouse liver.

Xenotransplantation, such as from pigs to humans, could potentially compensate for the lack of human organ and tissue donors. Our results indicate that, in addition to potential immunological rejection, the transplanted cells or tissues may fail to interact appropriately with the host environment. We propose that the h-chimeric mouse is a useful model for not only examining the mechanism of liver regeneration but also studying risks of xenotransplantation.

## Acknowledgments

We thank Yasumi Yoshizane, Hiromi Kohno, Yoko Matsumoto, and Sanae Nagai for technical assistance and Dr. Masumi Yamada for helpful discussion and comments.

## References

1. Heckel JL, Sandgren EP, Degen JL, Palmiter RD, Brinster RL: Neonatal bleeding in transgenic mice expressing urokinase-type plasminogen activator. Cell 1990, 62:447–456
2. Locaputo S, Carrick TL, Bezerra JA: Zonal regulation of gene expression during liver regeneration of urokinase transgenic mice. Hepatology 1999, 29:1106–1113
3. Rhim JA, Sandgren EP, Degen JL, Palmiter RD, Brinster RL: Replacement of diseased mouse liver by hepatic cell transplantation. Science 1994, 263:1149–1152
4. Rhim JA, Sandgren EP, Palmiter RD, Brinster RL: Complete reconstitution of mouse liver with xenogeneic hepatocytes. Proc Natl Acad Sci USA 1995, 92:4942–4946
5. Dandri M, Burda MR, Gocht A, Török E, Pollok JM, Rogler CE, Will H, Petersen J: Woodchuck hepatocytes remain permissive for hepadnavirus infection and mouse liver repopulation after cryopreservation. Hepatology 2001, 34:824–833
6. Dandri M, Burda MR, Török E, Pollok JM, Iwanska A, Sommer G, Rogiers X, Rogler CE, Gupta S, Will H, Greten H, Petersen J: Repopulation of mouse liver with human hepatocytes and in vivo infection with hepatitis B virus. Hepatology 2001, 33:981–988
7. Tateno C, Yoshizane Y, Saito N, Kataoka M, Utoh R, Yamasaki C, Tachibana A, Soeno Y, Asahina K, Hino H, Asahara T, Yokoi T, Furukawa T, Yoshizato K: Near completely humanized liver in mice shows human-type metabolic responses to drugs. Am J Pathol 2004, 165:901–912
8. Meuleman P, Libbrecht L, De Vos R, de Hemptinne B, Gevaert K, Vandekerckhove J, Roskams T, Leroux-Roels G: Morphological and biochemical characterization of a human liver in an uPA-SCID mouse chimera. Hepatology 2005, 41:847–856
9. Emoto K, Tateno C, Hino H, Amano H, Imaoka Y, Asahina K, Asahara T, Yoshizato K: Efficient in vivo xenogeneic retroviral vector-mediated gene transduction into human hepatocytes. Hum Gene Ther 2005, 16:1168–1674
10. Kam I, Lynch S, Svanas G, Todo S, Polimeno L, Francavilla A, Penkrot RJ, Takaya S, Ericzon BG, Starzl TE, Van Thiel DH: Evidence that host size determines liver size: studies in dogs receiving orthotopic liver transplants. Hepatology 1987, 7:362–366
11. Van Thiel DH, Gavaler JS, Kam I, Francavilla A, Polimeno L, Schade RR, Smith J, Diven W, Penkrot RJ, Starzl TE: Rapid growth of an intact human liver transplanted into a recipient larger than the donor. Gastroenterology 1987, 93:1414–1419
12. Francavilla A, Zeng Q, Polimeno L, Carr BI, Sun D, Porter KA, Van Thiel DH, Starzl TE: Small-for-size liver transplantation into large recipient: a model of hepatic regeneration. Hepatology 1994, 19:210–216
13. Nakamura T, Tomita Y, Hirai R, Yamaoka K, Kaji K, Ichihara A: Inhibitory effect of transforming growth factor-β on DNA synthesis of adult rat hepatocytes in primary culture. Biochem Biophys Res Commun 1985, 133:1042–1050
14. Russell WE, Coffey RJ Jr., Ouellette AJ, Moses HL: Type β transforming growth factor reversibly inhibits the early proliferative response to partial hepatectomy in the rat. Proc Natl Acad Sci USA 1988, 85:5126–5130
15. Zhang YQ, Kanzaki M, Mashima H, Mine T, Kojima I: Norepinephrine reverses the effects of activin A on DNA synthesis and apoptosis in cultured rat hepatocytes. Hepatology 1996, 23:288–293
16. Hu PP, Datto MB, Wang XF: Molecular mechanisms of transforming growth factor-β signaling. Endocr Rev 1998, 19:349–363
17. Kumar A, Novoselov V, Celeste AJ, Wolfman NM, ten Dijke P, Kuehn MR: Nodal signaling uses activin and transforming growth factor-β receptor-regulated Smads. J Biol Chem 2001, 276:656–661
18. Braun L, Mead JE, Panzica M, Mikumo R, Bell GI, Fausto N: Transforming growth factor β mRNA increases during liver regeneration: a possible paracrine mechanism of growth regulation. Proc Natl Acad Sci USA 1988, 85:1539–1543
19. Romero-Gallo J, Sozmen EG, Chytil A, Russell WE, Whitehead R, Parks WT, Holdren MS, Her MF, Gautam S, Magnuson M, Moses HL, Grady WM: Inactivation of TGF-β signaling in hepatocytes results in an increased proliferative response after partial hepatectomy. Oncogene 2005, 24:3028–3041
20. Oe S, Lemmer ER, Conner EA, Factor VM, Levéen P, Larsson J, Karlsson S, Thorgeirsson SS: Intact signaling by transforming growth factor β is not required for termination of liver regeneration in mice. Hepatology 2004, 40:1098–1105
21. Hino H, Tateno C, Sato H, Yamasaki C, Katayama S, Kohashi T, Aratani A, Asahara T, Dohi K, Yoshizato K: A long-term culture of human hepatocytes which show a high growth potential and express

their differentiated phenotypes. Biochem Biophys Res Commun 1999, 256:184–191
22. Seglen PO: Preparation of isolated rat liver cells. Methods Cell Biol 1976, 13:29–83
23. Utoh R, Tateno C, Yamasaki C, Hiraga N, Kataoka M, Shimada T, Chayama K, Yoshizato K: Susceptibility of chimeric mice with livers repopulated by serially subcultured human hepatocytes to hepatitis B virus. Hepatology 2008, 47:435–446
24. Livak KJ, Schmittgen TD: Analysis of relative gene expression data using real-time quantitative PCR and the $2^{-\Delta\Delta C_T}$ method. Methods 2001, 25:402–408
25. Wack KE, Ross MA, Zegarra V, Sysko LR, Watkins SC, Stolz DB: Sinusoidal ultrastructure evaluated during the revascularization of regenerating rat liver. Hepatology 2001, 33:363–378
26. Martinez-Hernandez A, Delgado FM, Amenta PS: The extracellular matrix in hepatic regeneration. Localization of collagen types I, III, IV, laminin, and fibronectin. Lab Invest 1991, 64:157–166
27. Keppler D, Konig J: Hepatic canalicular membrane 5: expression and localization of the conjugate export pump encoded by the MRP2 (cMRP/cMOAT) gene in liver. FASEB J 1997, 11:509–516
28. Michalopoulos GK: Liver regeneration. J Cell Physiol 2007, 213: 286–300
29. Chari RS, Price DT, Sue SR, Meyers WC, Jirtle RL: Down-regulation of transforming growth factor beta receptor type I, II, and III during liver regeneration. Am J Surg 1995, 169:126–132
30. Weinstein M, Monga SP, Liu Y, Brodie SG, Tang Y, Li C, Mishra L, Deng CX: Smad proteins and hepatocyte growth factor control parallel regulatory pathways that converge on β1-integrin to promote normal liver development. Mol Cell Biol 2001, 21:5122–5131
31. Cassiman D, Libbrecht L, Desmet V, Denef C, Roskams T: Hepatic stellate cell/myofibroblast subpopulations in fibrotic human and rat livers. J Hepatol 2002, 36:200–209
32. Koniaris LG, McKillop IH, Schwartz SI, Zimmers TA: Liver regeneration. J Am Coll Surg 2003, 197:634–659
33. Patijn GA, Lieber A, Schowalter DB, Schwall R, Kay MA: Hepatocyte growth factor induces hepatocyte proliferation in vivo and allows for efficient retroviral-mediated gene transfer in mice. Hepatology 1998, 28:707–716
34. Huang W, Ma K, Zhang J, Qatanani M, Cuvillier J, Liu J, Dong B, Huang X, Moore DD: Nuclear receptor–dependent bile acid signaling is required for normal liver regeneration. Science 2006, 312:233–236
35. Derynck R, Akhurst RJ, Balmain A: TGF-β signaling in tumor suppression and cancer progression. Nat Genet 2001, 29:117–129
36. Jeruss JS, Sturgis CD, Rademaker AW, Woodruff TK: Down-regulation of activin, activin receptors, and Smads in high-grade breast cancer. Cancer Res 2003, 63:3783–3790
37. Masumoto N, Tateno C, Tachibana A, Utoh R, Morikawa Y, Shimada T, Momisako H, Itamoto T, Asahara T, Yoshizato K: GH enhances proliferation of human hepatocytes grafted into immunodeficient mice with damaged liver. J Endocrinol 2007, 194:529–553

Biochemical and Biophysical Research Communications 391 (2010) 316–321

Contents lists available at ScienceDirect

Biochemical and Biophysical Research Communications

journal homepage: www.elsevier.com/locate/ybbrc

# Suppression of type I collagen production by microRNA-29b in cultured human stellate cells

Tomohiro Ogawa [a], Masashi Iizuka [a], Yumiko Sekiya [a,b], Katsutoshi Yoshizato [a,c], Kazuo Ikeda [d], Norifumi Kawada [a,*]

[a] Department of Hepatology, Graduate School of Medicine, Osaka City University, Osaka, Japan
[b] Toray Industries Inc., Kanagawa, Japan
[c] PhoenixBio Co. Ltd., Hiroshima, Japan
[d] Department of Functional Anatomy, Graduate School of Medicine, Nagoya City University, Aichi, Japan

ARTICLE INFO

*Article history:*
Received 6 November 2009
Available online 12 November 2009

*Keywords:*
Liver fibrosis
SP1
TGF-β
Interferon
TargetScan

ABSTRACT

MicroRNAs (miRNAs) are small noncoding RNAs that regulate gene expression through imperfect base pairing with the 3′ untranslated region (3′UTR) of target mRNA. We studied the regulation of alpha 1 (I) collagen (Col1A1) expression by miRNAs in human stellate cells, which are involved in liver fibrogenesis. Among miR-29b, -143, and -218, whose expressions were altered in response to transforming growth factor-β1 or interferon-α stimulation, miR-29b was the most effective suppressor of type I collagen at the mRNA and protein level via its direct binding to Col1A1 3′UTR. miR-29b also had an effect on SP1 expression. These results suggested that miR-29b is involved in the regulation of type I collagen expression by interferon-α in hepatic stellate cells. It is anticipated that miR-29b will be used for the regulation of stellate cell activation and lead to antifibrotic therapy.



## Introduction

Hepatic stellate cells, which reside in the Disse's space outside the liver sinusoids, maintain a quiescent phenotype and store vitamin A under physiological conditions [1,2]. When liver injury occurs due to alcohol abuse, hepatitis viral infection, or obesity, stellate cells activate in response to inflammatory stimuli and become myofibroblastic cells that express smooth muscle α-actin as a representative marker [2]. Myofibroblastic cells secrete profibrogenic mediators, such as transforming growth factor-β (TGF-β), connective tissue growth factor, and tissue inhibitor of matrix metalloproteinases, and generate extracellular matrix materials including collagens, fibronectin, and laminin; thus, they play a pivotal role in liver fibrogenesis [3]. In particular, collagen production by activated stellate cells is regulated by TGF-β in an autocrine loop, which is accompanied by the induction of TGF-β receptors [4]. Suppression of hepatic stellate cell activation and collagen expression is thus a critical issue to establish therapeutic strategies for human liver fibrosis [1,5].

MicroRNAs (miRNAs) are endogenous small noncoding RNAs that modulate gene expression through imperfect base pairing with the 3′ untranslated region (UTR) of target mRNA, resulting in the inhibition of translation or the promotion of mRNA degradation [6,7]. miRNAs play roles in cell proliferation [8], development [9], and differentiation [10], and their contribution to human diseases such as cancer, cardiomyopathies, and schizophrenia have been reported [11–13]. miR-122 is also involved in the defense system against viral hepatitis C with regard to interferon (IFN)-β therapy [14], and miR-26 expression status is associated with survival and response to adjuvant IFNα therapy in patients with hepatocellular carcinoma [15]. Some miRNAs are involved in liver development and hepatocyte lipid metabolism [16–18].

Recent studies have shown that miRNAs are additionally involved in the alteration of hepatic stellate cell phenotypes; down-regulation of miR-27a and -27b allows culture-activated rat stellate cells to return to a quiescent phenotype with abundant vitamin A storage and decreased cell proliferation [19]; miR-15b and -16, which target the Bcl-2 and caspase signaling pathways, may affect stellate cell activation and liver fibrosis [20]. However, the function of miRNAs in hepatic stellate cell activation and their collagen production is largely unknown.

Here, we show that miR-29b, which is induced in human stellate cells (LX-2) treated with IFNα, is a potential regulator of type I collagen mRNA and protein expression. Although the primary action of IFNs is to eradicate viruses, i.e., hepatitis B and C viruses in

*Abbreviations:* Col1A1, alpha 1 (I) collagen; DMEM, Dulbecco's modified Eagle's medium; FBS, fetal bovine serum; IFN, interferon; miRNAs, microRNAs; TGF-β, transforming growth factor-β; UTR, untranslated region.

* Corresponding author. Address: Department of Hepatology, Graduate School of Medicine, Osaka City University, 1-4-3, Asahimachi, Abeno, Osaka 545-8585, Japan. Fax: +81 6 6646 9072.
*E-mail address:* kawadanori@med.osaka-cu.ac.jp (N. Kawada).

0006-291X/$ - see front matter © 2009 Elsevier Inc. All rights reserved.
doi:10.1016/j.bbrc.2009.11.056

the case of the liver, IFNs also exhibit an antifibrotic action in human chronic hepatitis [21,22] and rodent liver fibrosis models [23]. Our data suggest that miR-29b may be a novel regulator of type I collagen expression in addition to its involvement in the well-known Smad cascade. Moreover, miR-29b upregulation may play a partial role in the antifibrotic action of IFNs.

## Materials and methods

*Materials.* Recombinant human TGF-β1 was purchased from PeproTech (London, UK). Human natural IFNα was obtained from Otsuka Pharmaceutical Co. (Tokushima, Japan). Precursors of miR-29b, -143, and -218, and the negative control were purchased from Ambion (Austin, TX, USA). Dulbecco's modified Eagle's medium (DMEM) and fetal bovine serum (FBS) were purchased from Sigma Chemical Co. (St. Louis, MO, USA). Rabbit monoclonal antibodies against Smad2 and phospho-Smad2 were purchased from Cell Signaling Technology Inc. (Beverly, MA, USA). The mouse monoclonal antibody against SP1 was purchased from Bio Matrix Research Inc. (Chiba, Japan). Rabbit polyclonal antibody against type I collagen was purchased from Rockland Immunochemicals, Inc. (Gilbertsville, PA, USA). Mouse monoclonal antibody against GAPDH was purchased from Chemicon International Inc. (Temecula, CA, USA). Enhanced Chemiluminescence plus detection reagent was purchased from GE Healthcare (Buckinghamshire, UK). Immobilon P membranes were purchased from Millipore Corp. (Bedford, MA, USA). All other reagents were purchased from Sigma Chemical Co. or Wako Pure Chemical Co. (Osaka, Japan).

*Preparation of the human hepatic stellate cell line LX-2.* The human hepatic stellate cell line (LX-2, donated by Dr. Scott Friedman), which was spontaneously immortalized by growth in low serum, was established as reported previously [24]. Characterizations of the cells are described in detail elsewhere. The cells were maintained on plastic culture plates in DMEM supplemented with 10% FBS. After the culture had continued for the indicated number of days, the medium was replaced with DMEM supplemented with 0.1% FBS plus test agents, and the culture was continued for another 24 h.

*Quantitative real-time PCR.* Total RNA was extracted from human stellate cells using the miRNeasy Mini Kit (Qiagen, Valencia, CA, USA). cDNAs were synthesized using 0.5 μg of total RNA, ReverTra Ace (Toyobo, Osaka, Japan), and oligo(dT)$_{12-18}$ primers according to the manufacturer's instructions [25]. Gene expression was measured by real-time PCR using cDNA, real-time PCR Master Mix Reagents (Toyobo), and a set of gene-specific oligonucleotide primers (alpha 1 (I) collagen [Col1A1]: Forward 5′-CCCGGGTTTCAGAGACA ACTTC-3′, Reverse 5′-TCCACATGCTTTATTCCAGCAATC-3′; TGF-β1: Forward 5′-AGCGACTCGCCAGAGTGGTTA-3′, Reverse 5′-GCAGTG TGTTATCCCTGCTGTCA-3′; SP1: Forward 5′-TCGGATGAGCTACA GAGGCACAA-3′, Reverse 5′-GTCACTCCTCATGAAGCGCTTAGG-3′; and GAPDH: Forward 5′-GCACCGTCAAGGCTGAGAAC-3′, Reverse 5′-TGGTGAAGACGCCAGTGGA-3′) with an Applied Biosystems Prism 7500 (Applied Biosystems, Foster City, CA, USA). To detect miRNA expression, the RT reaction was performed using the TaqMan MicroRNA Assay (Applied Biosystems) according to the manufacturer's instructions. The GAPDH level was measured and used to normalize the relative abundance of mRNAs and miRNAs.

*Immunoblot.* Proteins (20–50 μg) were subjected to sodium dodecyl sulfate–polyacrylamide gel electrophoresis and then transferred onto Immobilon P membranes. After blocking, the membranes were treated with primary antibodies, followed by peroxidase-conjugated secondary antibodies. Immunoreactive bands were visualized by the enhanced chemiluminescence system using the Fujifilm Image Reader LAS-3000 (Fuji Medical Systems, Stamford, CT, USA).

*Transient transfection of miRNA precursors.* Precursors of miR-29b, -143, and -218, and the negative control were transfected into human stellate cells using Lipofectamine 2000 (Invitrogen, Carlsbad, CA, USA) at a final concentration of 50 nM. Briefly, the cells were plated in DMEM supplemented with 10% FBS at a density of 1–2 × 10$^5$ cells/ml 24 h prior to the transfection. miRNA precursors and Lipofectamine 2000 were mixed at a ratio of 25 (pmol):1 (μl) in Opti-MEM I Reduced Medium (Invitrogen) and incubated for 20–30 min at room temperature. The miRNA precursor–Lipofectamine 2000 complexes were then added to stellate cell culture medium. After 6 h, the culture medium was changed, and TGF-β1 was added at a concentration of 2 ng/ml.

*Luciferase reporter assay.* 3′UTRs containing putative miRNA target regions of the Col1A1 and SP1 genes were obtained by PCR using human stellate cell cDNA as a template and primer sets as follows: Col1A1–miR-29: Forward 5′-TTCTCGAGGTTCTTGTCTTG ATGTGTCACC-3′, Reverse 5′-TTTCTAGAGAGAGCAGAGGCCTGAGA AG-3′; Col1A1–miR-143: Forward 5′-CTCGAGACTCCCTCCATCCCAA CCT-3′, Reverse 5′-TCTAGAATTGCTGGGCAGACAATAC-3′; Col1A1–miR-218: Forward 5′-CTCGAGGTGGATGGGGACTTGTGAAT-3′, Reverse 5′-TCTAGATTATGTTTGGGTCATTTCCAC-3′; SP1–miR-29: Forward 5′-TTCTCGAGTGGGTGCTACACAGAATGC-3′, Reverse 5′-TTTC TAGAAGACTGTCCTTATTTCCTTGGTA-3′; and SP1–miR-218: Forward 5′-CTCGAGGATGTTTTCCCTTAACTTTTCCT-3′, Reverse 5′-TCT AGACTAAAAGCTTATATCCTCAGCATC-3′. Each of the forward and reverse primers carried the *Xho*I and *Xba*I sites at their 5′-ends. The obtained DNA fragments were inserted into the pmirGLO Vector (Promega, San Luis Obispo, CA, USA). The resulting vectors were dubbed pCol1A1–miR-29/mirGLO, pCol1A1–miR-143/mirGLO, pCol1A1–miR-218/mirGLO, pSP1–miR-29/mirGLO, and pSP1–miR-218/mirGLO. Human stellate cells were seeded on 96-well plates (Microtest 96-well Assay Plate; Becton Dickinson, Franklin Lakes, NJ, USA) in DMEM supplemented with 10% FBS at a density of 2 × 10$^4$ cells/well. The following day, they were transfected with 200 ng of reporter plasmid along with miRNA precursors using Lipofectamine 2000 as described above and incubated for an additional 24 h. After incubation, the medium was removed from the wells, and 20 μl of phosphate-buffered saline was added. The Dual-Glo Luciferase Assay System (Promega) was used to analyze luciferase expression according to the manufacturer's protocol. Firefly luciferase activity was normalized to *Renilla* luciferase activity to adjust for variations in transfection efficiency among experiments.

*Statistical analysis.* Data presented as bar graphs are the means ± SD of at least three independent experiments. Statistical analysis was performed using Student's *t*-test, and $P < 0.05$ was considered significant.

## Results and discussion

### *Regulation of Col1A1 expression by TGF-β1 and IFNα in human stellate cells*

Immortalized human stellate cells, LX-2, are classified as an activated phenotype that expresses mRNAs for Col1A1 and other fibrogenetic molecules and are reported to be highly gene-transfectable [24]. At first, we observed that Col1A1 mRNA expression increased dose-dependently by TGF-β1 (Fig. 1A), whereas this upregulation was significantly inhibited by the presence of 100 IU/ml of human IFNα (Fig. 1B).

### *Extraction of miR-29b, -143, and -218 as candidates interacting with Col1A1 3′UTR*

To determine the role of miRNAs in human stellate cell collagen expression, we searched for predictable miRNAs that could interact

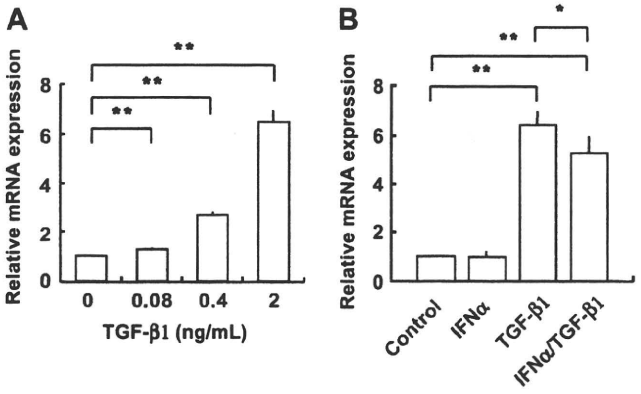


**Fig. 1.** Regulation of alpha 1 (I) collagen (Col1A1) expression in human stellate cells. (A) Dose-dependent effect of TGF-β1 on Col1A1 mRNA expression. Human stellate cells, LX-2, were treated with TGF-β1 (0, 0.08, 0.4, and 2 ng/ml) for 24 h in DMEM containing 0.1% FBS. (B) Effect of IFNα on Col1A1 mRNA expression in human stellate cells stimulated with TGF-β1. The cells were treated with IFNα (100 IU/ml), TGF-β1 (2 ng/ml), or IFNα (100 IU/ml) + TGF-β1 (2 ng/ml) for 24 h in DMEM containing 0.1% FBS. Control: human stellate cells were cultured for 24 h in DMEM containing 0.1% FBS. mRNA expression was analyzed by real-time PCR. The results are expressed as relative expression against control expression without treatment. $^{*}P < 0.05$; $^{**}P < 0.01$.

with 3′UTR of human Col1A1 mRNA using TargetScan Human Release 5.1 (http://www.targetscan.org/). As a result, miR-29, -98, -129, -133, -143, -196, -218, and let-7 were extracted as candidates. Because further *in silico* analyses among the eight candidates indicated that miR-29b, -143, and -218 were highly homologous to the Col1A1 3′UTR, we checked the expression levels of these miRNAs in human stellate cells by real-time PCR. As a result, miR-143 and -218 expressions were up and downregulated dose-dependently by TGF-β1, respectively, (Fig. 2A and B). Although miR-29b expression was unaffected by TGF-β1, it increased in

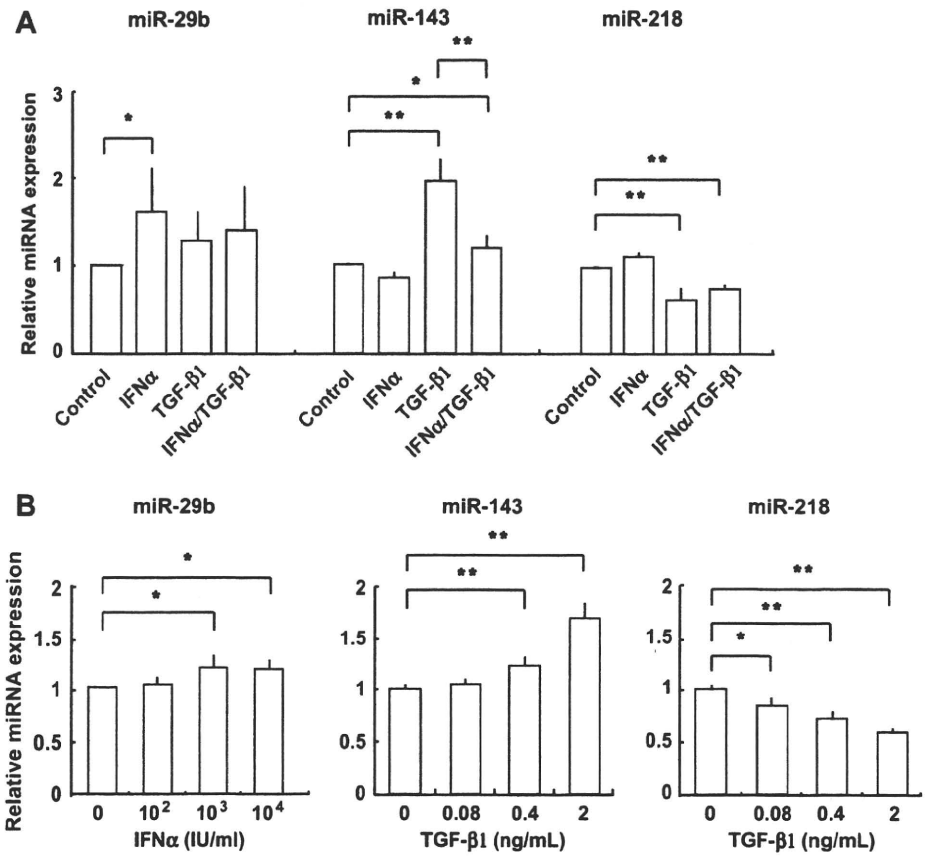


**Fig. 2.** Expression of miR-29b, -143, and -218 in human stellate cells. (A) Expression of miR-29b, -143, and -218 in human stellate cells, LX-2. The cells were treated with IFNα (100 IU/ml), TGF-β1 (2 ng/ml), or IFNα (100 IU/ml) + TGF-β1 (2 ng/ml) for 24 h in DMEM containing 0.1% FBS. Control: human stellate cells were cultured for 24 h in DMEM containing 0.1% FBS. (B) Dose-dependent effect of IFNα or TGF-β1 on the expression of miR-29b, -143, and -218 in human stellate cells. miRNA expression was analyzed by real-time PCR. The results are expressed as relative expression against control expression without treatment. $^{*}P < 0.05$; $^{**}P < 0.01$.

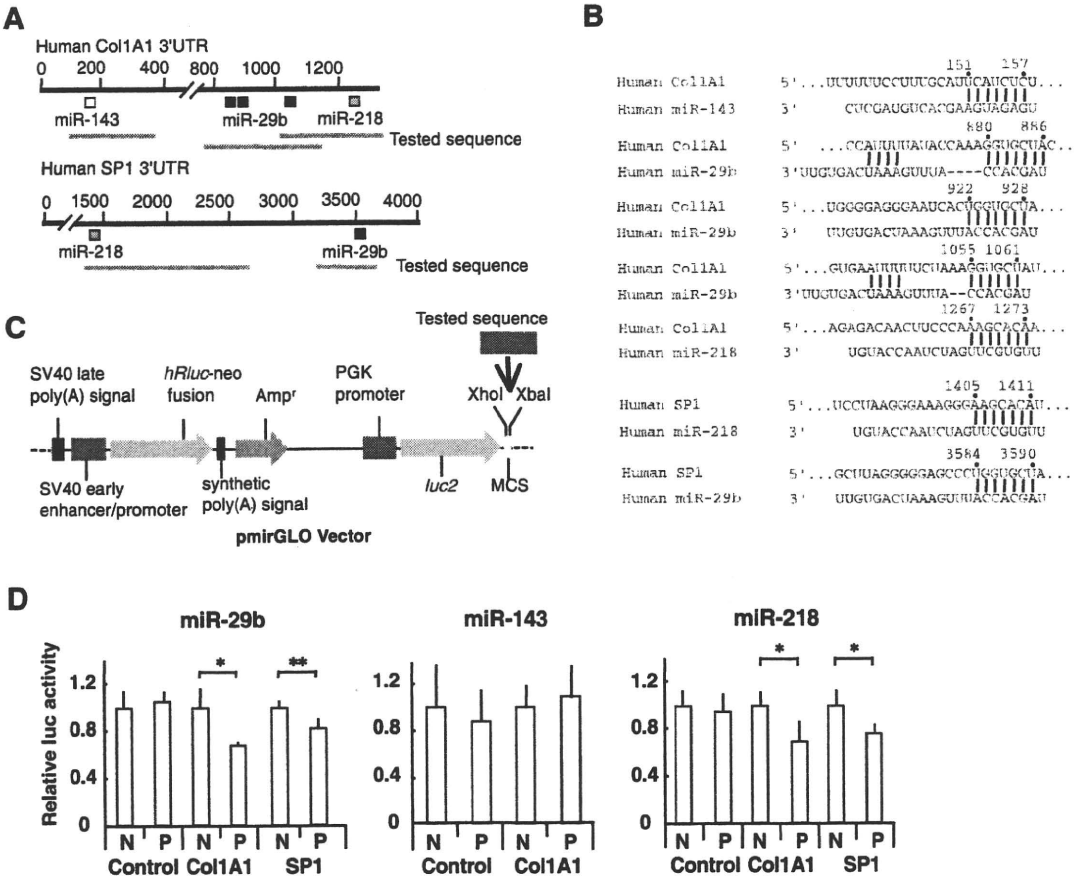


**Fig. 3.** Interaction of miR-29b, -143, and -218 with the 3′UTRs of alpha 1 (I) collagen (Col1A1) and SP1 mRNAs. (A) Schematic indication of the miRNA binding sites in the 3′UTRs of Col1A1 and SP1 mRNAs based on TargetScan Human Release 5.1 (http://www.targetscan.org/). Each black, white, and gray box indicates miR-29b, -143, and -218, respectively. Tested sequences indicate the regions that were inserted into the luciferase reporter vector. (B) Predicted consequential pairing of the target region and miRNAs. Arabic numerals above indicate the positions relative to the 3′UTR start sites. (C) Luciferase reporter vector structure. The vector contained two expression units; one for the *Renilla* luciferase gene (*hRluc*-neo fusion) expression. This unit was driven by an SV40 early promoter. The other was for the firefly luciferase gene (*luc2*). This unit was driven by a human phosphoglycerate kinase (PGK) promoter and contained multiple cloning sites (MCS) downstream of the *luc2* sequence. Each Col1A1 and SP1 3′UTR containing a putative miRNA target region (tested sequence) was cloned into the MCS. Arrows indicate the gene directions. $Amp^R$ indicates an ampicillin-resistant plasmid gene. (D) Interaction of miR-29b, -143, and -218 with the 3′UTRs of Col1A1 and SP1 mRNAs in human stellate cells. Relative luciferase activity derived from pCol1A1–miR-29/mirGLO and pSP1–miR-29/mirGLO in the presence of miR-29b precursors (left panel), pCol1A1–miR-143/mirGLO in the presence of miR-143 precursors (center panel), and pCol1A1–miR-218/mirGLO and pSP1–miR-218/mirGLO in the presence of miR-218 precursors (right panel). The pmirGLO vector was used as a negative control reporter vector (control). N: cotransfection of reporter vectors along with negative control precursors, which have a scrambled sequence. P: cotransfection of reporter vectors along with miRNA precursors. Firefly and *Renilla* luciferase activities were determined, and firefly luciferase was normalized to *Renilla* luciferase activity. Results are expressed as relative activities against the activity in the presence of negative control precursors. $^{*}P < 0.05$ and $^{**}P < 0.01$.

the presence of IFNα (Fig. 2A and B). Thus, we assumed that these miRNAs might affect type I collagen expression via their interaction with Col1A1 3′UTR in human stellate cells.

### *Interaction of miR-29b, -143, and -218 with 3′UTRs of Col1A1 and SP1 mRNAs*

The prediction of miRNA target regions on Col1A1 3′UTR by TargetScan indicated that Col1A1 3′UTR has three target regions for miR-29b, one for miR-143, and one for miR-218 (Fig. 3A and B). Because collagen gene expression is regulated by miR-192 via an interaction with the transcriptional repressor E-box [26], we additionally considered SP1, which is a transcriptional regulator of Col1A1 expression induced by TGF-β1 [27,28]. The predicted miRNA target regions of SP1 3′UTR contained one target region for miR-29b and one for miR-218 (Fig. 3A and B).

To investigate the direct targeting of Col1A1 by miR-29b, -143, and -218 and that of SP1 by miR-29b and -218, the sequence of each target region was cloned and inserted into the downstream region of the firefly luciferase reporter gene (Fig. 3C). The resulting vectors were dubbed pCol1A1–miR-29/mirGLO, pCol1A1–miR-143/mirGLO, pCol1A1–miR-218/mirGLO, pSP1–miR-29/mirGLO, and pSP1–miR-218/mirGLO. These vectors were cotransfected into human stellate cells with miRNA precursors. As a result, the miR-29b and -218 precursors inhibited luciferase activity derived from the vectors carrying Col1A1 or SP1 3′UTRs (Fig. 3D). In contrast, the miR-143 precursors had no effect on luciferase activity of the vector carrying Col1A1 3′UTR (Fig. 3D). According to these observations, we assumed that the Col1A1 and SP1 3′UTR sequences could be targeted by miR-29b and -218, whereas miR-143, which was induced by TGF-β1 (Fig. 2A and B), had a negligible effect on Col1A1 expression in human stellate cells.

### *Regulation of type I collagen expression by miR-29b and -218*

Next, we examined the effect of miR-29b and -218 overexpression on type I collagen mRNA and protein expression in human stellate cells. Transient transfection of miR-29b precursors signifi-

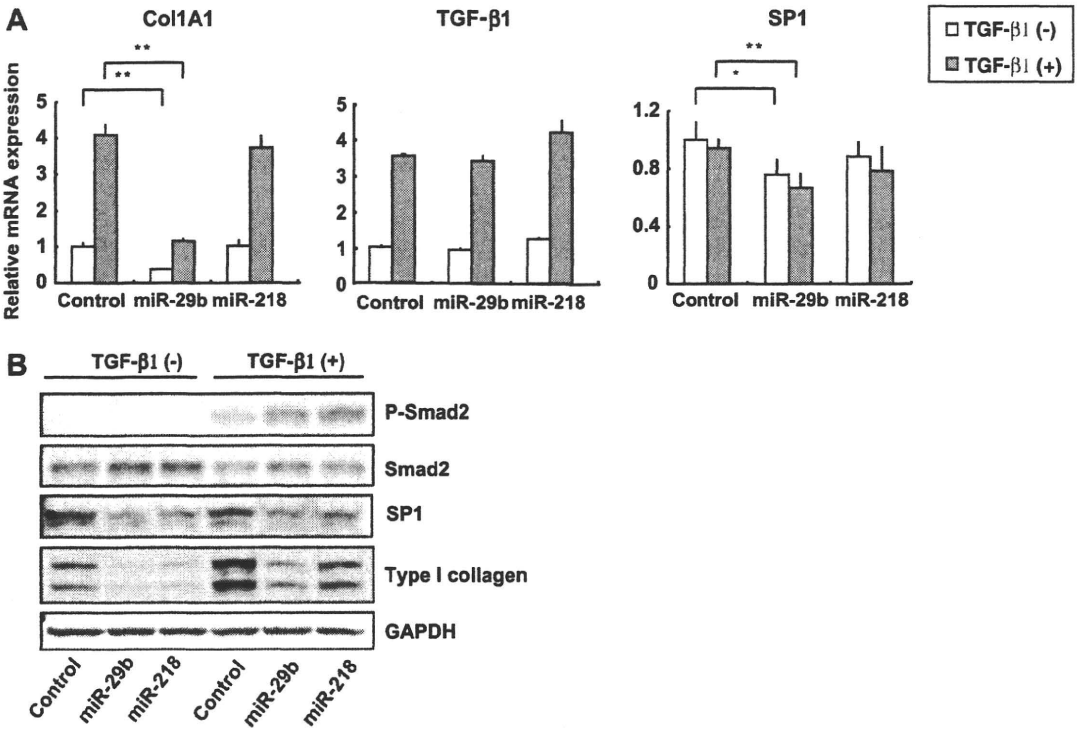


**Fig. 4.** Effect of miR-29b and -218 on type I collagen expression in human stellate cells. Human stellate cells were cultured in DMEM supplemented with 10% FBS and were transfected with 50 nM miR-29b, -218 precursors, or a negative control, which had a scrambled sequence (control) using Lipofectamine 2000. After 6 h, the medium was changed to DMEM containing 0.1% FBS with or without 2 ng/ml TGF-β1, and the culture was continued for another 24 h. (A) Effect of miR-29b and -218 precursors on the expression of Col1A1, TGF-β1, and SP1 mRNAs in human stellate cells with (gray column) or without (white column) TGF-β1. mRNA expression was analyzed by real-time PCR. The results are expressed as relative expression against control expression. $^{*}P < 0.05$; $^{**}P < 0.01$. (B) Effect of miR-29b and -218 precursors on the protein expression of phospho-Smad2 (P-Smad2), Smad2, SP1, type I collagen, and GAPDH in human stellate cells in the presence (+) or absence (−) of TGF-β1.

cantly inhibited type I collagen mRNA and protein expression (Fig. 4A, left panel, and B) in unstimulated human stellate cells. Additionally, transfection of miR-29b precursors completely suppressed the upregulation of type I collagen mRNA and protein under TGF-β1 stimulation. TGF-β1 stimulation induces Col1A1 mRNA expression through a pathway that includes SP1 and phosphorylated Smad2/3 [29]. In our results, upregulation of TGF-β1 mRNA (Fig. 4A, center panel) and phosphorylation of Smad2 (Fig. 4B) under TGF-β1 stimulation were unaffected by the transfection of miR-29b precursors. These results suggested that miR-29b may affect the downstream of phosphorylated Smad2. Moreover, the transfection of miR-29b precursors decreased SP1 mRNA and protein expression (Fig. 4A, right panel, and B). Thus, the miR-29b-induced repression of type I collagen expression could be caused by its direct interaction with Col1A1 3′UTR and additionally by its interaction with SP1 expression in human stellate cells. These observations agree with a report showing the role of miR-29 in collagen expression and cardiac fibrosis after cardiac infarction [30]. In contrast, transfection of miR-218 precursors triggered a negligible change in Col1A1 and SP1 mRNA expression (Fig. 4A, left and right panels) but slightly reduced their protein level (Fig. 4B). Taken together, these results imply that miR-29b is the most potent miRNA with regard to collagen production in human stellate cells.

## Conclusions

We found a potent repression of collagen production by miR-29b in human stellate cells. IFNs attenuate and may regress liver fibrosis caused by hepatitis C viral infection [21–23], although the precise molecular mechanism has yet to be demonstrated. The present study using human stellate cells demonstrated that IFNα upregulates miR-29b (Fig. 2B and C), which is a negative regulator of type I collagen production via the interaction with Col1A1 and SP1 3′UTRs. This observation implies the contribution of miR-29b to antifibrotic IFN actions. Targeted delivery of miR-29b to activated stellate cells in the liver could become a new therapeutic strategy for human liver fibrosis in the future.

## Acknowledgment

This work was supported by a grant from the Ministry of Health, Labour and Welfare of Japan to N. Kawada (2008–2009).

## References

[1] R. Bataller, D.A. Brenner, Hepatic stellate cells as a target for the treatment of liver fibrosis, Semin. Liver Dis. 21 (2001) 437–451.
[2] S.L. Friedman, Molecular regulation of hepatic fibrosis, an integrated cellular response to tissue injury, J. Biol. Chem. 275 (2000) 2247–2250.
[3] N. Kawada, The hepatic perisinusoidal stellate cell, Histol. Histopathol. 12 (1997) 1069–1080.
[4] S. Dooley, B. Delvoux, B. Lahme, K. Mangasser-Stephan, A.M. Gressner, Modulation of transforming growth factor beta response and signaling during transdifferentiation of rat hepatic stellate cells to myofibroblasts, Hepatology 31 (2000) 1094–1106.
[5] E. Albanis, S.L. Friedman, Hepatic fibrosis. Pathogenesis and principles of therapy, Clin. Liver Dis. 5 (2001) 315–334. v–vi.
[6] W. Filipowicz, S.N. Bhattacharyya, N. Sonenberg, Mechanisms of post-transcriptional regulation by microRNAs: are the answers in sight?, Nat Rev. Genet. 9 (2008) 102–114.
[7] D.P. Bartel, MicroRNAs: genomics, biogenesis, mechanism, and function, Cell 116 (2004) 281–297.
[8] J. Brennecke, D.R. Hipfner, A. Stark, R.B. Russell, S.M. Cohen, Bantam encodes a developmentally regulated microRNA that controls cell proliferation and regulates the proapoptotic gene hid in *Drosophila*, Cell 113 (2003) 25–36.

[9] G.M. Schratt, F. Tuebing, E.A. Nigh, C.G. Kane, M.E. Sabatini, M. Kiebler, M.E. Greenberg, A brain-specific microRNA regulates dendritic spine development, Nature 439 (2006) 283–289.
[10] C.Z. Chen, L. Li, H.F. Lodish, D.P. Bartel, MicroRNAs modulate hematopoietic lineage differentiation, Science 303 (2004) 83–86.
[11] J. Kota, R.R. Chivukula, K.A. O'Donnell, E.A. Wentzel, C.L. Montgomery, H.W. Hwang, T.C. Chang, P. Vivekanandan, M. Torbenson, K.R. Clark, J.R. Mendell, J.T. Mendell, Therapeutic microRNA delivery suppresses tumorigenesis in a murine liver cancer model, Cell 137 (2009) 1005–1017.
[12] J.F. Chen, E.P. Murchison, R. Tang, T.E. Callis, M. Tatsuguchi, Z. Deng, M. Rojas, S.M. Hammond, M.D. Schneider, C.H. Selzman, G. Meissner, C. Patterson, G.J. Hannon, D.Z. Wang, Targeted deletion of Dicer in the heart leads to dilated cardiomyopathy and heart failure, Proc. Natl. Acad. Sci. USA 105 (2008) 2111–2116.
[13] D.O. Perkins, C.D. Jeffries, L.F. Jarskog, J.M. Thomson, K. Woods, M.A. Newman, J.S. Parker, J. Jin, S.M. Hammond, MicroRNA expression in the prefrontal cortex of individuals with schizophrenia and schizoaffective disorder, Genome Biol. 8 (2007) R27.
[14] I.M. Pedersen, G. Cheng, S. Wieland, S. Volinia, C.M. Croce, F.V. Chisari, M. David, Interferon modulation of cellular microRNAs as an antiviral mechanism, Nature 449 (2007) 919–922.
[15] J. Ji, J. Shi, A. Budhu, Z. Yu, M. Forgues, S. Roessler, S. Ambs, Y. Chen, P.S. Meltzer, C.M. Croce, L.X. Qin, K. Man, C.M. Lo, J. Lee, I.O. Ng, J. Fan, Z.Y. Tang, H.C. Sun, X.W. Wang, MicroRNA expression, survival, and response to interferon in liver cancer, N. Engl. J. Med. 361 (2009) 1437–1447.
[16] C.E. Rogler, L. Levoci, T. Ader, A. Massimi, T. Tchaikovskaya, R. Norel, L.E. Rogler, MicroRNA-23b cluster microRNAs regulate transforming growth factor-beta/bone morphogenetic protein signaling and liver stem cell differentiation by targeting Smads, Hepatology 50 (2009) 575–584.
[17] C. Esau, S. Davis, S.F. Murray, X.X. Yu, S.K. Pandey, M. Pear, L. Watts, S.L. Booten, M. Graham, R. McKay, A. Subramaniam, S. Propp, B.A. Lollo, S. Freier, C.F. Bennett, S. Bhanot, B.P. Monia, MiR-122 regulation of lipid metabolism revealed by in vivo antisense targeting, Cell Metab. 3 (2006) 87–98.
[18] L. Zheng, G.C. Lv, J. Sheng, Y.D. Yang, Effect of miRNA-10b in regulating cellular steatosis level by targeting PPAR-alpha expression, a novel mechanism for the pathogenesis of NAFLD, J. Gastroenterol. Hepatol. (2009).
[19] J. Ji, J. Zhang, G. Huang, J. Qian, X. Wang, S. Mei, Over-expressed microRNA-27a and 27b influence fat accumulation and cell proliferation during rat hepatic stellate cell activation, FEBS Lett. 583 (2009) 759–766.
[20] C.J. Guo, Q. Pan, D.G. Li, H. Sun, B.W. Liu, MiR-15b and miR-16 are implicated in activation of the rat hepatic stellate cell: an essential role for apoptosis, J. Hepatol. 50 (2009) 766–778.
[21] Y. Shiratori, F. Imazeki, M. Moriyama, M. Yano, Y. Arakawa, O. Yokosuka, T. Kuroki, S. Nishiguchi, M. Sata, G. Yamada, S. Fujiyama, H. Yoshida, M. Omata, Histologic improvement of fibrosis in patients with hepatitis C who have sustained response to interferon therapy, Ann. Intern. Med. 132 (2000) 517–524.
[22] T. Poynard, J. McHutchison, G.L. Davis, R. Esteban-Mur, Z. Goodman, P. Bedossa, J. Albrecht, Impact of interferon alfa-2b and ribavirin on progression of liver fibrosis in patients with chronic hepatitis C, Hepatology 32 (2000) 1131–1137.
[23] Y. Inagaki, T. Nemoto, M. Kushida, Y. Sheng, K. Higashi, K. Ikeda, N. Kawada, F. Shirasaki, K. Takehara, K. Sugiyama, M. Fujii, H. Yamauchi, A. Nakao, B. De Crombrugghe, T. Watanabe, I. Okazaki, Interferon alfa down-regulates collagen gene transcription and suppresses experimental hepatic fibrosis in mice, Hepatology 38 (2003) 890–899.
[24] L. Xu, A.Y. Hui, E. Albanis, M.J. Arthur, S.M. O'Byrne, W.S. Blaner, P. Mukherjee, S.L. Friedman, F.J. Eng, Human hepatic stellate cell lines, LX-1 and LX-2: new tools for analysis of hepatic fibrosis, Gut 54 (2005) 142–151.
[25] K. Otogawa, T. Ogawa, R. Shiga, K. Nakatani, K. Ikeda, Y. Nakajima, N. Kawada, Attenuation of acute and chronic liver injury in rats by iron-deficient diet, Am. J. Physiol. Regul. Integr. Comp. Physiol. 294 (2008) R311–R320.
[26] M. Kato, J. Zhang, M. Wang, L. Lanting, H. Yuan, J.J. Rossi, R. Natarajan, MicroRNA-192 in diabetic kidney glomeruli and its function in TGF-beta-induced collagen expression via inhibition of E-box repressors, Proc. Natl. Acad. Sci. USA 104 (2007) 3432–3437.
[27] L. Li, C.M. Artlett, S.A. Jimenez, D.J. Hall, J. Varga, Positive regulation of human alpha 1 (I) collagen promoter activity by transcription factor Sp1, Gene 164 (1995) 229–234.
[28] I. Garcia-Ruiz, P. de la Torre, T. Diaz, E. Esteban, I. Fernandez, T. Munoz-Yague, J.A. Solis-Herruzo, Sp1 and Sp3 transcription factors mediate malondialdehyde-induced collagen alpha 1 (I) gene expression in cultured hepatic stellate cells, J. Biol. Chem. 277 (2002) 30551–30558.
[29] P. Sysa, J.J. Potter, X. Liu, E. Mezey, Transforming growth factor-beta1 up-regulation of human alpha(1) (I) collagen is mediated by Sp1 and Smad2 transacting factors, DNA Cell Biol. 28 (2009) 425–434.
[30] E. van Rooij, L.B. Sutherland, J.E. Thatcher, J.M. DiMaio, R.H. Naseem, W.S. Marshall, J.A. Hill, E.N. Olson, Dysregulation of microRNAs after myocardial infarction reveals a role of miR-29 in cardiac fibrosis, Proc. Natl. Acad. Sci. USA 105 (2008) 13027–13032.

HUMAN GENE THERAPY 21:40–50 (January 2010)

DOI: 10.1089/hum.2009.027

# *In Vivo* Stable Transduction of Humanized Liver Tissue in Chimeric Mice via High-Capacity Adenovirus–Lentivirus Hybrid Vector

Shuji Kubo,[1,2] Miho Kataoka,[3] Chise Tateno,[3] Katsutoshi Yoshizato,[3,4] Yoshiko Kawasaki,[2] Takahiro Kimura,[1] Emmanuelle Faure-Kumar,[1] Donna J. Palmer,[5] Philip Ng,[5] Haruki Okamura,[2] and Noriyuki Kasahara[1]

**Abstract**

We developed hybrid vectors employing high-capacity adenovirus as a first-stage carrier encoding all the components required for *in situ* production of a second-stage lentivirus, thereby achieving stable transgene expression in secondary target cells. Such vectors have never previously been tested in normal tissues, because of the scarcity of suitable *in vivo* systems permissive for second-stage lentivirus assembly. Here we employed a novel murine model in which endogenous liver tissue is extensively reconstituted with engrafted human hepatocytes, and successfully achieved stable transduction by the second-stage lentivirus produced *in situ* from first-stage adenovirus. This represents the first demonstration of the functionality of adenoviral-lentiviral hybrid vectors in a normal parenchymal organ *in vivo*.

## Introduction

ADENOVIRAL VECTORS (AdVs) have been successfully used *in vivo* to transduce various postmitotic tissues, but generally only transient gene expression can be achieved because of cytotoxic T-lymphocyte–mediated immune responses against viral genes retained in conventional AdVs, and their extremely low frequency of chromosomal integration (Harui *et al.*, 1999; Wivel *et al.*, 1999). More persistent expression can be maintained by high-capacity, helper-dependent AdVs (HDAdVs) from which all of the viral coding sequences have been removed (Parks *et al.*, 1996; Schiedner *et al.*, 1998; Kochanek, 1999; Kim *et al.*, 2001; Oka *et al.*, 2001), but its duration is still limited because of progressive dilution of the extrachromosomal HDAdV vector DNA as transduced cells divide. Treatment of hereditary diseases may require more stable, long-term transgene expression, which can be achieved only through permanent integration or ongoing episomal replication of vector DNA.

To overcome this limitation, various hybrid vector systems have been developed, which employ AdV as a first-stage delivery vehicle to efficiently enter target cells, but then utilize the machinery of integrating viruses or mobile genetic elements to achieve permanent chromosomal integration (Feng *et al.*, 1997; Caplen *et al.*, 1999; Lieber *et al.*, 1999; Recchia *et al.*, 1999; Tan *et al.*, 1999; Leblois *et al.*, 2000; Soifer *et al.*, 2001; Soifer *et al.*, 2002; Yant *et al.*, 2002; Kubo and Mitani, 2003; Dorigo *et al.*, 2004; Picard-Maureau *et al.*, 2004). Efficient two-stage transduction *in vitro* and stable long-term transgene expression have previously been demonstrated with AdV–transposon (Soifer *et al.*, 2001; Yant *et al.*, 2002), AdV–adeno-associated virus (Lieber *et al.*, 1999; Recchia *et al.*, 1999), AdV–retrovirus (Feng *et al.*, 1997; Caplen *et al.*, 1999; Soifer *et al.*, 2002), AdV–foamy virus (Picard-Maureau *et al.*, 2004), and AdV–lentivirus (Kubo and Mitani, 2003) vectors. In particular, Kubo and Mitani (2003) have demonstrated the ability of an AdV–lentivirus hybrid vector to efficiently enter a variety of cell types via the first-stage HDAdV and subsequently mediate *in situ* production of a human immunodeficiency virus (HIV)-derived second-stage lentiviral vector (LV), which then stably delivers a marker gene to neighboring cells. However, this hybrid vector generated second-stage LV pseudotyped with the vesicular stomatitis virus G glycoprotein (VSV-G), a highly fusogenic and toxic envelope

[1]Division of Digestive Diseases, Department of Medicine, University of California at Los Angeles, Los Angeles, CA 90095.
[2]Laboratory of Host Defenses, Institute for Advanced Medical Sciences, Hyogo College of Medicine, Nishinomiya, Hyogo 663-8501, Japan.
[3]Yoshizato Project, CLUSTER, Hiroshima Prefectural Institute of Industrial Science and Technology, Higashi-Hiroshima, Hiroshima 739-0046, Japan.
[4]Developmental Biology Laboratory and Hiroshima University 21st Century COE Program for Advanced Radiation Casualty Medicine, Department of Biological Science, Graduate School of Science, Higashi-Hiroshima, Hiroshima 739-8526, Japan.
[5]Center for Cell & Gene Therapy, Baylor College of Medicine, Houston, TX 77030.

protein (Ory *et al.*, 1996), which may result in unwanted cytotoxic effects in the primary target cells during LV production. Further, the ability of AdV-lentivirus hybrid vectors to stably transduce normal quiescent tissues *in vivo* has never previously been tested.

We have now developed an improved high-capacity AdV-lentivirus hybrid vector system, designated HL, and examined the ability of this new hybrid system to mediate efficient and stable gene transfer *in vitro* and *in vivo*. The first-stage HDAdV of the HL hybrid system directs the production of a minimal second-stage LV that retains less than 800 bp of HIV sequence (Chen *et al.*, 2002) and is pseudotyped with the murine leukemia virus (MLV) 4070A amphotropic envelope, which is much less cytotoxic than VSV-G. However, to test the transduction efficiency of the new HL hybrid vector system, target cells that can support *in situ* production of the HIV-derived second-stage LV are required. For *in vitro* experiments, human cell lines permissive for HIV replication can be employed. However, the requirement for human target cells presents a challenge to testing the functionality of the HL hybrid vector system *in vivo*, particularly with respect to its ability to stably transduce normal organs and tissues.

As nearly 90% of the input dose of AdV introduced *in vivo* accumulates in the liver upon intravenous injection (Kass-Eisler *et al.*, 1994; Huard *et al.*, 1995; Kubo *et al.*, 1997), and nearly 100% transduction of hepatocytes can be achieved at higher doses (Li *et al.*, 1993), the liver is an attractive target for *in vivo* testing of the HL system. However, multiple blocks to HIV replication have been reported in rodent cells, including cellular entry, reduced abundance of unspliced HIV-RNA and *gag* proteins, and defects in infectious particle assembly (Hofmann *et al.*, 1999; Bieniasz and Cullen, 2000; Mariani *et al.*, 2000). Therefore, to test the HL hybrid vector *in vivo*, we sought a humanized liver model that is permissive for HIV particle assembly.

Successful reconstitution of human liver tissue has recently been achieved in immunodeficient mice (Dandri *et al.*, 2001; Mercer *et al.*, 2001). Dandri *et al.* (2001) reported that cross-breeding of recombinant activation gene-2–deleted mice with transgenic mice expressing the hepatotoxic urokinase-type plasminogen activator (uPA) results in immunodeficient progeny which undergo progressive liver degeneration. These progeny were successfully transplanted with human hepatocytes, resulting in chimeric liver tissue with a replacement index of up to 15%, rendering these mice permissive for HBV infection (Dandri *et al.*, 2001). Similarly, Mercer *et al.* (2001) demonstrated that uPA/SCID mice bearing chimeric humanized livers with replacement index values of 50% could support HCV replication (Dandri *et al.*, 2001). More extensive repopulation has been difficult to achieve, likely because engrafted human hepatocytes produce complement factors, which appear to exert lethal effects in mice with higher replacement values. However, Tateno *et al.* (2004) and Yoshizato and colleagues (2004) have recently demonstrated that administration of a C5/C3 convertase inhibitor successfully rescued uPA/SCID mice whose chimeric livers proved to be almost completely repopulated with human hepatocytes exhibiting normal cytoarchitecture. The transduction efficiency of oncoretroviral vectors has previously been tested in this humanized liver model, and consistent with their inability to enter quiescent postmitotic cells, was found to be in the order of 5% (Emoto *et al.*, 2005). We have now utilized this unique chimeric liver model to test the ability of the HL hybrid system to mediate efficient entry by the first-stage HDAdV, *in situ* production of the second-stage LV, and stable transduction in fully humanized livers *in vivo*. To our knowledge, this represents the first report of *in vivo* testing of an AdV–lentivirus hybrid vector system in a normal parenchymal organ.

## Materials and Methods

### *Cells*

Cell lines including 293 (Graham *et al.*, 1977) (Microbix, Toronto, Canada), 293T (DuBridge *et al.*, 1987), and the Gli36 human glioma (Sena-Esteves *et al.*, 2000) were cultured in Dulbecco's modified Eagle's medium supplemented with 10% fetal calf serum (FCS; Omega, Tarzana, CA). Hep3B human hepatocellular carcinoma cells were cultured in Eagle's minimum essential medium supplemented with 10% FCS, 1 m*M* sodium pyruvate, and nonessential amino acids. Primary human hepatocytes and their specific medium were purchased from Cambrex (Baltimore, MD; CC-2591).

### *HL first-stage HDAdV construction and production*

The phosphoglycerokinase promoter-driven green fluorescence protein (GFP) marker gene cassette, cytomegalovirus promoter (CMV)-driven *gag/pol/rev* lentiviral packaging cassette, simian virus 40 early promoter-driven MLV 4070A amphotropic envelope cassette, and minimal LV construct (Robbins *et al.*, 1998; Chen *et al.*, 2002) were sequentially cloned into the HDAdV plasmid pSTK120, which contains the human Ad5 inverted terminal repeat sequences and packaging signal, resulting in the construction of the complete HL vector plasmid, pHL. Additional details regarding the pHL construct, and the HIV-based minimal LV contained therein, are provided upon request.

The HL vector and control HDAdV cmv-GFP (Ad GFP) were prepared using the FLPe/*FRT* helper virus system (Umana *et al.*, 2001). The vectors were titrated on 293 cells for GFP expression, using a FACScalibur flow cytometer (Becton Dickinson, San Jose, CA), on day 2 post-infection, defined as transducing units per ml (TU/ml). Another control HDAdV, HDΔ28E4LacZ, was prepared as previously described (Palmer and Ng, 2003). Helper virus contamination levels were determined by Southern blot, as previously described (Kubo and Mitani, 2003).

### *Second-stage LV production after infection with HL first-stage HDAdV*

To confirm production of LV in cells (Gli36, HeLa, Hep3B, HepG2 and human primary hepatocytes) infected by the HL vector, $4\times10^5$ cells of each were infected with various amounts of HL vector. The amount of vector used for each infection was based on the titer determined using each cell line. At 4 hr postinfection, the infected cells were washed three times with phosphate-buffered saline (PBS), and incubated in growth medium. At 48 hr postinfection, the virus-containing medium was harvested, centrifuged, filtered through a 0.45-$\mu$m pore filter, and used for titration on 293 cells by X-galactosidase (gal) staining to detect $\beta$gal expression. In preliminary experiments, the level of residual adenovirus carried over in the filtered supernatant medium after infection of primary cells at a multiplicity of infection (MOI) of 10, as

measured by flow cytometry for GFP expression in secondary cells, was less than 1%.

To inhibit lentiviral infection, 293 cells were infected with the viral supernatant in the presence or absence of 5 $\mu M$ zidovudine (AZT; Sigma, St. Louis, MO).

To investigate the kinetics of LV vector production after HL vector infection, $4\times10^5$ Hep3B cells were infected with HL at various MOIs in six-well plates. The medium was collected at different time points and titrated on 293 cells, as described earlier.

### *Long-term culture experiments*

Hep3B cells ($2\times10^5$) were infected with the HL vector, at an MOI of 10, and incubated in the presence of AZT on a 10-cm dish. The cells were split at a ratio of 1:20 once a week, and expression of GFP was examined by flow cytometry. At each passage, DNA was extracted from a portion of the cells and analyzed for proviral integration by Southern hybridization. A part of the HL-infected cells were also plated on Lab-Tek chamber slides (Thermo Fisher Scientific, Rochester, NY). The next day, the cells were fixed for 10 min with 4% paraformaldehyde, washed with PBS, and incubated with 50 m$M$ $NH_4Cl$ in PBS for 5 min. The cells were permeabilized in 0.5% Triton/PBS for 5 min and then incubated for 30 min in 1% bovine serum albumin/PBS for blocking. The cells were incubated for 1 hr with a 1:1000 dilution of mouse anti-GFP monoclonal (Chemicon, Temecula, CA). Immunoreactivity for GFP was visualized with a 1:5000 dilution of goat anti-mouse immunoglobulin G (IgG) (H + L) Alexa Fluor 488. The cells were then incubated with a 1:1000 dilution of rabbit anti-$\beta$gal polyclonal (ab616; Abcam, Cambridge, MA). Immunoreactivities for $\beta$gal were visualized with a 1:5000 dilution of goat anti-rabbit IgG (H + L) Alexa Fluor 594 (Molecular Probes, Eugene, OR).

### *Animals*

Chimeric mice with human liver were generated as previously described (Tateno *et al.*, 2004). Briefly, uPA/SCID mice were generated by crossing uPA mice [B6SJL-TgN(Alb1Plau)144Bri; The Jackson Laboratory, Bar Harbor, ME] with SCID mice (Fox Chase SCID C.B-17/Icr-*scid* Jcl; Clea Japan, Tokyo, Japan). The $uPA^{+/+}SCID^{+/+}$ mice were screened by polymerase chain reaction (PCR) and injected with $5.0–7.5\times10^5$ viable human hepatocytes (IVT079; In Vitro Technologies Inc., Baltimore, MD) through a small left-flank incision into the inferior splenic pole at 20–30 days after birth. The mice were injected intraperitoneally with 200 $\mu$l of 1.5 mg/ml Futhan (nafamostat mesilate, 6-amidino-2-naphthyl *p*-guanidinobenzoate dimethanesulfonate; gift from Torii Pharmaceutical, Tokyo, Japan) to enhance repopulation of the liver with human hepatocytes. The replacement index was estimated by serum level of human albumin as previously described (Tateno *et al.*, 2004). Generally, >5 mg/ml human albumin in the blood indicates high replacement index values of >70%, and mice screened in this manner were used for experiments at 6–8 weeks posttransplantation.

After injection with gadolinium (10 mg/kg body weight) to eliminate Kupffer cells (Lieber *et al.*, 1997), either HL vector ($2\times10^9$ TU/200 ml) or buffer (PBS) was injected via tail vein, followed by sacrifice at 4 days or 4 weeks postinfection ($n=4$ per group). A portion of each liver sample was immediately digested into cell suspensions and used for flow cytometric analysis. The remaining portion was frozen in liquid nitrogen for isolation of genomic DNA or for frozen tissue sections. Immunofluorescence (IF) and immunohistochemistry (IHC) for GFP were performed on frozen liver sections using standard methods with GFP-specific antibodies (ab290; Abcam): goat anti-rabbit IgG-Alexa Fluor 488 for IF, or Vectastain ABC kit (Vector Laboratories, Burlingame, CA) and diaminobenzidine for IHC. IF for $\beta$gal was also performed using rabbit anti-$\beta$gal antibodies (ab616; Abcam) and goat anti-rabbit IgG-Alexa Fluor 594, as earlier. X-gal staining using standard methods was also performed on glutaraldehyde-fixed liver sections, and the proportion of $\beta$gal-positive cells was determined by image analysis using the SPOT digital imaging system and NIH ImageJ software (version 1.34). The replacement index of the mouse liver with human hepatocytes was also determined by IHC for human-specific cytokeratin-8 and -18 (CK8/18) as previously described (Tateno *et al.*, 2004) and is defined as the ratio of area occupied by human hepatocytes to the entire area examined. To assess any potential hepatotoxicity, sera were collected from mice at the time of scheduled sacrifice, that is, at 4 weeks after injection with HL vector or PBS, and serum levels of aspartate amino transferase (AST) were measured by automated colorimetric assay.

### *Molecular analysis of integrated LVs in the liver*

High-molecular-weight genomic DNA was extracted from livers injected with HL vector or PBS. For detection of the stably integrated form of the second-stage LV after production from the first-stage HDAdV, high-molecular-weight genomic DNA (500 ng) was subjected to nested PCR to amplify lentiviral integration events close to or within *Alu* repeat sequences in the human genome (Nguyen *et al.*, 2002; Serafini *et al.*, 2004). Briefly, the first PCR (PCR1) was carried out using a sense oligomer specific for the conserved sequences of human *Alu* (*Alu*-s; 5′-TCCCAGCTACTCGGGA GGCTGAGG-3′) and an antisense oligomer specific for the PBS region of HIV-1 upstream of *gag* (5NC2-as; 5′-GAGTC CTGCGTCGAGAGAG-3′). All amplifications were done using 100 $\mu$l of reaction mixture containing 200 ng of genomic DNA, 0.4 m$M$ of each dNTP, 0.8 $\mu M$ of each sense and antisense primer, 5% dimethyl sulfoxide, and 2 U *Taq* DNA polymerase. After the first DNA denaturation at 95°C for 5 min, 30 amplification cycles were performed consisting of denaturation for 1 min at 94°C, annealing for 1 min at 60°C, and extension for 3 min at 72°C. One aliquot (1:100 dilution) of the first PCR products was subjected to a second PCR (PCR2) amplification using the nested primers, LTR9-s (5′-GCCTCAATAAAGCTTGCCTTG-3′) and U5PBS-as (spanning the U5LTR/PBS boundary region) (5′-GGCGCCAC TGCTAGAGATTTT-3′), which amplified a fragment of 121 bp. The nested PCR conditions were similar to those of the first amplification, except for an annealing temperature of 55°C and an extension time of 1 min. Twenty amplification cycles were performed. In control reactions, genomic DNA that had not been subjected to the first round of PCR was also amplified using the second PCR primers to exclude the presence of residual nonintegrated vector DNA. As a loading control, the same DNA samples were subjected to a PCR that amplified a 610-bp region of human $\beta$-actin (5′-GATCAT GTTTGAGACCTTCA-3′ and the reverse sequence 5′-ACC

TTGATCTTCATGGTGC-3′), with the following amplification conditions: 95°C for 2 min, then 30 cycles of 95°C for 30 sec, 65°C for 30 sec, and 72°C for 1 min, followed by a final extension at 72°C for 5 min. Amplification products were resolved on 1.5% agarose gel containing ethidium bromide and detected by ultraviolet transillumination.

The copy number of the integrated form of the lentiviral construct in each cell was determined by quantitative real-time PCR (Q-PCR) with βgal-specific primers and probe, designed using Primer Express software V. 1.0 (Applied Biosystems, Foster City, CA). Primer and probe sequences spanned a 91-bp region in the βgal-coding region, consisting of the following sequences: forward primer, 5′-CTATCCC GACCGCCTTACTG-3′; reverse primer, 5′-GTTTTCGCTCG GGAAGACGTA-3′; probe, 5′-FAM-CAGCGGTCAAAA CAG-TAMRA-3′. Amplification was performed in a reaction volume of 25 μl under the following conditions: 300 ng of high-molecular-weight genomic DNA, 1×Taqman universal PCR master mix (Applied Biosystems), 600 n*M* forward primer, 900 n*M* reverse primer, and 100 n*M* probe. Thermal cycling conditions were 2 min incubation at 50°C, 10 min at 95°C, followed by 40 cycles of successive incubation at 95°C for 15 sec and 60°C for 1 min. Standard curves were generated using serial dilutions of HL vector plasmid, pHL, from 5 to 50,000,000 copies in a background of 50,000 equivalents (300 ng) of untransduced genomic DNA from the chimeric mouse liver. Duplicate samples were amplified in an ABI Prism 7700 sequence detector with continuous fluorescence monitoring. Data were collected and analyzed using 7700 Sequence Detection System software v.1.6.3. (Applied Biosystems). The copy number per cell of integrated lentiviral construct was calculated as the average copy number divided by 50,000 cells (equivalent to 300 ng genomic DNA).

### *Statistical analysis*

The results are presented as mean ± standard deviation. Statistical significance of differences was calculated using Student's *t*-test, and a *p*-value of $<0.01$ was considered significant.

## Results

### *Design and production of the HL hybrid vector*

The hybrid vector HL contains a complete set of HIV-derived lentiviral packaging components incorporated into an HDAdV (Fig. 1A), including (1) a multiple attenuated packaging construct expressing *gag-pol*, *rev*, and the *rev* response element sequence, (2) an envelope construct expressing amphotropic (i.e., broad mammalian host range) *env* from MLV strain 4070A, and (3) a minimal HIV-based LV transfer vector encoding a βgal marker gene driven by a methylation-resistant MLV promoter (MND promoter) (Chen *et al.*, 2002). As this transfer vector sequence contains a LV packaging signal so that its mRNA will be encapsidated by the coexpressed packaging and envelope components to form LV virions, the βgal transgene will not only be expressed in cells directly infected by the HDAdV, but also be transmitted to adjacent cells. The adenoviral backbone

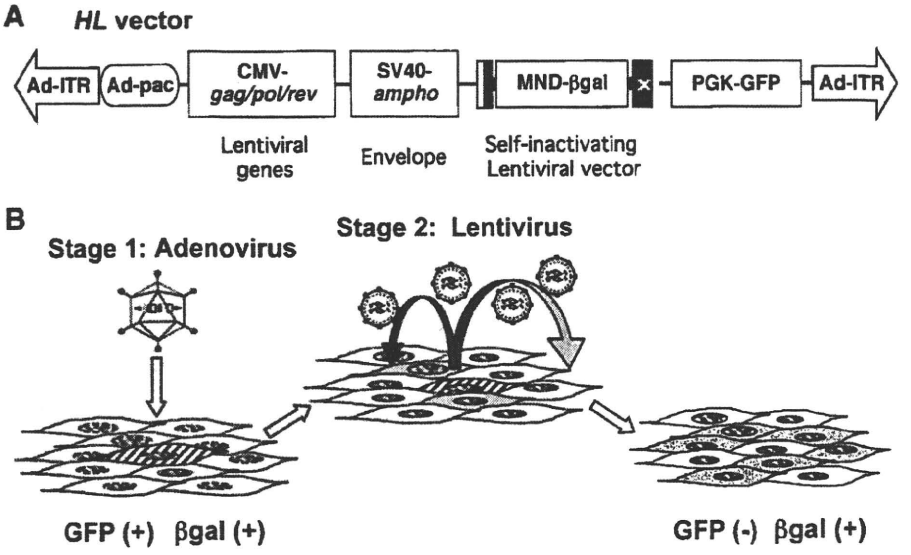


**FIG. 1.** Outline of the high-capacity adenovirus/lentivirus hybrid vector (HL vector) system. (**A**) Schematic structure of the HL vector. An HL vector is a helper-dependent adenoviral vector encoding expression cassettes for production of a lentiviral vector (LV) based on human immunodeficiency virus 1 (HIV-1). The HL vector has two inverted terminal repeats (Ad-ITR) and the packaging signal (Ad-pac) of human adenovirus type 5 and encodes four gene expression cassettes: (1) a self-inactivating minimal LV that contains the central polypurine tract, the woodchuck hepatitis virus posttranscriptional regulatory element, and the β-galactosidase gene (βgal) driven by the methylation-resistant murine leukemia virus LTR promoter (MND) (Robbins *et al.*, 1998; Chen *et al.*, 2002) as a marker; (2) HIV-*gag/pol/rev* coding sequences driven by cytomegalovirus (CMV) promoter; (3) the amphotropic murine leukemia virus envelope driven by the simian virus 40 early promoter (SV40) for pseudotyping of the lentivirus; and (4) the enhanced green fluorescent protein (GFP) driven by phosphoglycerokinase (PGK) promoter as a marker of the adenoviral backbone. (**B**) Two-stage transduction with the HL vector. The HL vector infects the initial target cells efficiently as an adenoviral vector and produces an LV *in situ*. The LV then infects surrounding secondary target cells and integrates into chromosomes for stable gene expression.

sequence also contains a GFP expression cassette unlinked to the LV components; the GFP marker gene will not be encapsidated into LV particles, thereby allowing specific quantitation of initial transduction by HDAdV itself. Thus, it is possible to distinguish between untransduced cells [GFP (−), βgal(−)], cells transduced by HL first-stage HDAdV only [GFP(+), βgal(+)], and cells transduced by HL second-stage LV [GFP(−), βgal(+)] (Fig. 1B).

The first-stage HDAdV was propagated using the FRT/FLPe helper system (Umana *et al.*, 2001). The GFP titers of purified HL vector preparations on 293 cells ranged from $4.1\times10^9$ to $1.8\times10^{10}$ TU/ml. Vector stocks contained less than 0.1% helper virus contamination, as determined by Southern hybridization, using a probe for the adenoviral packaging signal (data not shown).

### *Infection with HL first-stage HDAdV results in production of functional second-stage LV*

Following infection by the HL first-stage HDAdV vector at various MOIs, cell-free conditioned media from various human cell lines, including Gli36 (glioma), HeLa (cervical adenocarcinoma), and Hep3B and HepG2 (both hepatocellular carcinoma), were inoculated into fresh 293 cell cultures and tested for their ability to mediate secondary transmission of βgal expression. For all primary target cell lines tested, increasing MOI during first-stage HDAdV transduction correlated with increasing βgal transmission to secondary target cells (Fig. 2A). Further, βgal expression in secondary target cells was markedly suppressed by the reverse transcriptase inhibitor AZT, indicating that the observed transmission was indeed mediated by second-stage LV and was not due to carry-over of the first-stage HDAdV or pseudotransduction by overexpressed βgal protein (Fig. 2B). Of the cell lines tested, Gli36 and Hep3B produced the highest titers of LV ($1.0\times10^4$ and $5.1\times10^4$ TU/ml, respectively, at MOI = 100) (Fig. 2A), which also correlated with high levels of p24 production (236 and 316 ng/ml, respectively). Primary human hepatocytes also produced LV at titers of $6.0\times10^1$, $1.0\times10^3$, and $1.2\times10^4$ TU/ml upon infection with 1, 10, and 100 μl of HL vector ($4.0\times10^8$ TU/ml), respectively. Taken together, these findings indicate that the HL hybrid vector is

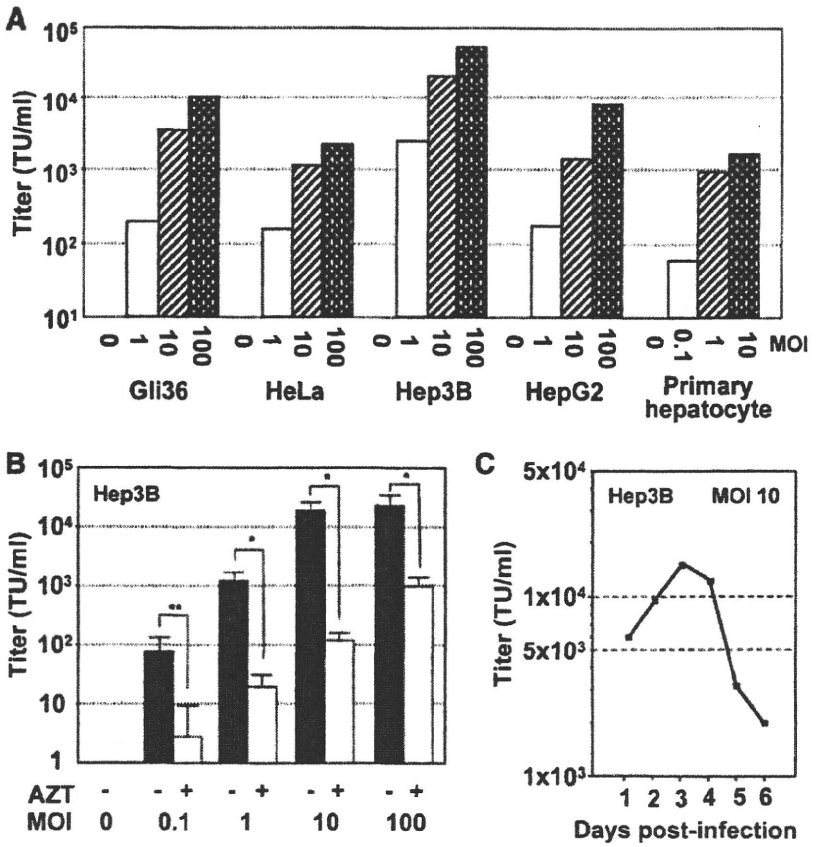


FIG. 2. Production of LV via HL vector system. (A) Production of LV in a variety of cell types after HL infection. Various cell lines indicated in the figure were infected with HL at multiplicity of infections (MOIs) of 1, 10, or 100. After 48 hr, viral supernatant was collected and titrated on 293 cells for βgal expression. (B) Production of LV following HL vector infection. Hep3B cells were infected with the HL vector at MOIs of 0.1, 1, 10, or 100. After 48 hr, viral supernatant was collected and titrated on 293 cells for βgal expression in the presence or absence of zidovudine (AZT, 5 μM). Data shown are average titers and standard deviations from the experiment performed in triplicate. Effect of AZT on titers was determined by Student's *t*-test (**$p < 0.05$, *$p < 0.01$). (C) Time course of lentiviral production from Hep3B cells infected with the HL vector. Hep3B cells were infected with HL at an MOI of 10 and monitored for up to 6 days. At different time points indicated in the figure, the medium was replaced, and the viral supernatant was titrated for βgal expression on 293 cells.

capable of directing the production of infectious LV particles from a variety of cell types, and that the LV yield is dependent upon the MOI and the target cell type.

To determine how long cells can produce LV after being infected with the HL first-stage HDAdV vector, a time-course experiment was performed. After infection of Hep3B cells with the HL first-stage HDAdV vector at an MOI of 10, the culture medium was harvested and replaced with fresh medium every day. The LV titers of the conditioned media harvested daily were measured on secondary target cells and were found to increase, reaching a peak level by day 3 post-HDAdV infection ($1.3\times10^4$ TU/ml; Fig. 2C). Thereafter, HL-infected human cells continued to sustain LV production for several days (postinfection day 6 titer – $2.0\times10^3$ TU/ml).

### In vitro *persistence of second-stage LV-transduced cells following HL first-stage HDAdV infection*

The spread of lentivirus in long-term cultures of HL-infected cells was examined by maintaining infected Hep3B in culture (Fig. 3A). As expected, GFP expression from the adenovirus backbone significantly decreased over time because of ongoing cell division-mediated dilution of HDAdV episomes in the culture. The percentage of GFP-positive cells

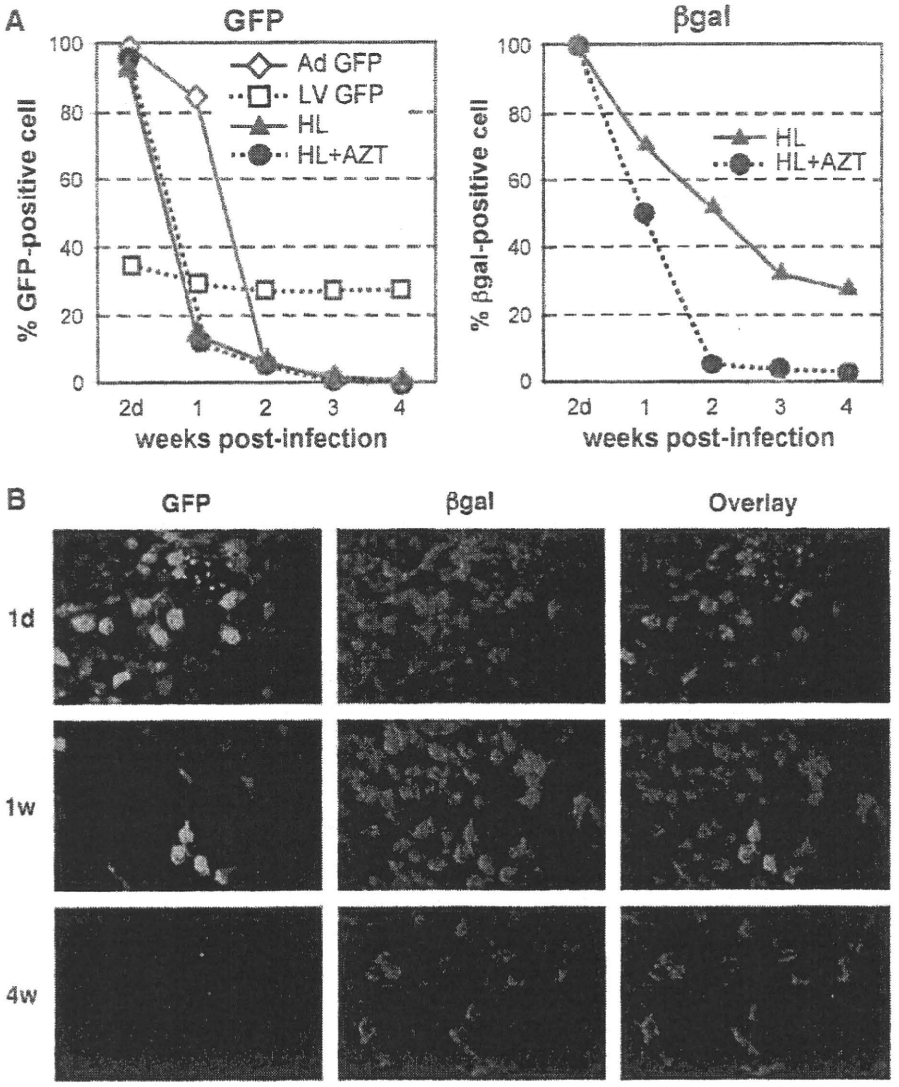


FIG. 3. Spread of LV-transduced cells and persistent gene expression following HL vector infection. (A) Transduction efficiencies of HL hybrid vector-infected cells. Hep3B cells ($2\times10^5$) infected with the HL vector at an MOI of 10 were incubated overnight, and the cells were split the following day and cultivated in the presence (blue circle) or absence (red triangle) of AZT on a 10-cm dish. The control samples infected with an LV GFP (brown square) or an Ad GFP (green diamond) are also shown. The cells were passaged at a ratio of 1:20 every week, and expressions of GFP and βgal were examined. Data are representative of three independent experiments, all yielding similar results. (B) Persistent gene expression achieved via HL hybrid vector system in transformed human hepatocytes *in vitro*. Hep3B cells were infected with HL vector at an MOI of 10. The cells were passaged at a ratio of 1:20 every week. Expressions of GFP and βgal were analyzed by immunofluorescence staining using anti-GFP and anti-βgal antibody at the indicated time points after HL infection.

quickly decreased from >90% to <2% within 2 weeks postinfection in the HL-infected cells (HL and HL + AZT) as well as in cells infected with control Ad GFP. Initially, a parallel decrease in βgal-positive cells was observed. However, 25% of the HL-infected cells (HL) remained βgal positive at 4 weeks postinfection, whereas those in the HL-infected/AZT-treated cells (HL + AZT) were <2% βgal positive within 2 weeks postinfection. Persistent βgal expression in the HL-infected cells (HL) was also confirmed by IF staining (Fig. 3B). Southern hybridization of high-molecular-weight genomic DNA extracted from the cells at week 4 confirmed LV proviral integration and a direct correlation between βgal expression and the copy number of the integrated βgal transgenes (data not shown). This also demonstrates that persistent βgal expression in the HL-infected cells is mediated by stable transduction with the HL second-stage LV vector.

### In vivo *persistence of second-stage LV-transduced cells in humanized liver following intravenous administration of HL first-stage HDAdV*

*In vivo* testing of the HL vector system requires a model that is permissive for assembly of human lentivirus. We employed a unique humanized model in which endogenous murine hepatocytes are extensively replaced with human hepatocytes. The replacement indices, calculated as the frequency of human-specific CK8/18-positive regions relative to that of the entire examined area in the mouse liver (Tateno *et al.*, 2004), ranged from 63.7% to 86.6% (Fig. 4A). This model was found to be efficiently transduced by control HDAdV (HDΔ28E4LacZ) (Palmer and Ng, 2003) (data not shown), and so chimeric uPA/SCID mice with highly humanized livers were intravenously injected with the HL first-stage HDAdV vector.

First, GFP expression from the adenoviral backbone of the HL first-stage HDAdV in liver tissue was analyzed by flow cytometry. The results showed 7.64% ± 1.33% GFP-positive cells at 4 days postinfection and 0.21% ± 0.07% GFP-positive cells at 4 weeks postinfection. This reduction in GFP-positive hepatocytes was also confirmed by IF (Fig. 4B) and IHC (Fig. 4C).

On the other hand, βgal expression persisted for at least 4 weeks postinfection as shown by IF studies (Fig. 4D) and X-gal tissue staining (Fig. 4E). Quantitation by image analysis revealed that the percentage of βgal-positive cells increased from 16.21% ± 3.70% at 4 days, to 28.40 ± 4.92% at 4 weeks postinfection ($p = 0.0074$). The persistence of βgal expression suggested that stable integration by the second-stage LV might have occurred. To demonstrate integration of second-stage LV in human hepatocyte genomic DNA *in vivo*, nested *Alu*–lentivirus PCR was performed (Nguyen *et al.*, 2002; Serafini *et al.*, 2004). In this assay, the first round of PCR was performed using a sense primer specific for human *Alu* sequences and another primer specific for the lentiviral 5′ noncoding region as the antisense primer (*Alu*-s and 5NC2-as, respectively; Fig. 5A). As LV vectors randomly integrate at multiple sites and repetitive *Alu* sequences are scattered throughout the human genome, the first reaction generated products with variable sizes (Fig. 5B, PCR1). The second round of PCR, using nested primers within the viral LTR and the viral primer binding site, respectively ("LTR9-s" sense and "U5 PBS-as" antisense primers, as depicted in Fig. 5A), generated the expected 140-bp product from transduced liver tissues, but not from untransduced control liver (Fig. 5B, PCR1 + PCR2). Genomic DNA from transduced cells subjected only to second-round PCR amplification did not yield any signal, validating the inability of the nested primers alone to amplify any residual episomal LV sequences and confirming the requirement for first-round amplification with the *Alu*–lentivirus primers to detect integrated proviruses (Fig. 5B, PCR2). Although this is not a quantitative assay, taken together these results do demonstrate integration of the lentiviral sequences into the genome of human hepatocytes *in vivo*.

For further quantitative assessment of the percentage of cells expressing βgal from the lentivirus vector component, Q-PCR was again performed, this time using high-molecular-weight genomic DNA from each of liver tissues as the template and with primers and probe specific for the βgal gene. The Q-PCR results demonstrated that the percentage of βgal-positive cells was 13.8–56.6% at 4 weeks postinfection, correlating with the data obtained by Xgal staining (28.40% ± 4.92%) (Fig. 4E). These results indicate that *in situ* production and spread of second-stage LV had occurred in the humanized livers of chimeric mice following systemic administration of the HL first-stage HDAdV, and taken together with the above finding that the first-stage HDAdV was undetectable at 4 weeks postinfection, it is likely that βgal expression at a later time point is derived almost entirely from the second-stage LV.

To assess any potential vector-related hepatotoxicity, serum AST levels were measured and compared between HL vector-injected and control PBS-injected mice. It should be noted that the levels of serum liver enzymes in the uPA/SICD-based chimeric mouse model are generally high because of the ongoing hepatic expression of uPA, which mediates progressive destruction of murine hepatocytes and thereby allows gradual engraftment of human hepatocytes. Notably, however, there was no significant difference in the serum AST levels between HL-injected mice (272.5 ± 154.5 U/l) and PBS-treated group (453.0 ± 79.3 U/l) ($p = 0.1546$). Consistent with these findings, liver histology showed no significant difference between PBS- and HL vector-treated livers. Taken together with the serum AST levels, this indicates that the HL vector does not cause significant liver toxicity. In addition, as noted earlier, serum levels of human albumin remained at high values (>5 mg/ml) throughout these experiments, and replacement indices remained at high levels, ranging from 63.7% to 86.6% (Fig. 4A), further indicating that the HL vector does not show any selective toxicity that would alter the proportion of human hepatocytes.

## Discussion

The liver has a variety of characteristics that make it a significant target for gene therapy (Ferry and Heard, 1998). As the liver is the site of essential metabolic pathways, it is involved in many inborn metabolic diseases. Moreover, because of its highly vascularized architecture and position as a portal to blood circulation, the liver can serve as a secretory organ for the systemic delivery of therapeutic proteins. Because of the fenestrated structure of its endothelium, the liver parenchyma is readily accessible to large molecules such as DNA or recombinant viruses via the blood stream. AdVs accumulate